This is the per reviewed version of the following article:

J. Dobrić, Y. Cai, B. Young, B. Rossi. Behaviour of duplex stainless steel bolted connections, Thin-Walled Structures, Volume 169, 108380, https://doi.org/10.1016/j.tws.2021.108380

Behaviour of duplex stainless steel bolted connections

Jelena Dobrić[1], Yancheng Cai[2], Ben Young[2], Barbara Rossi[3]

[1] University of Belgrade, Faculty of Civil Engineering, jelena@imk.grf.bg.ac.rs

[2] Department of Civil and Environmental Engineering, The Hong Kong Polytechnic University, Hong Kong

[3] University of Oxford, Department of Engineering Science, barbara.rossi@new.ox.ac.uk

Abstract

This study deals with the behaviour of duplex stainless steel bolted connections. The aim of the study is to respond to the question if the current stainless steel design specifications are able to predict the behaviour of such connections. Firstly, the net cross-section capacity of duplex stainless steel plates subjected to tensile loading are presented. They were conducted to obtain the stress-strain curves and tensile fracture behaviour used to support the finite element (FE) fracture simulations. Secondly, nonlinear FE models are developed for duplex stainless steel bolted connections subjected to tensile loading. The FE models are validated against experimental data in terms of load-displacement curves, failure modes and ultimate loads. Then, a numerical parametric study that consists of 133 duplex stainless steel grade EN 1.4162 bolted connection specimens is carried out. The failure modes of bolted connections are carefully examined, including combined tear out and bearing, bearing and net section, looking at the influence of parameters such as end distance, edge distance and spacing between the bolts in the connections. The results are compared to the design rules prescribed in the current stainless steel design specifications. Generally, it is found that the Australian/New Zealand (AS/NZS), American (SEI/ASCE) Specification and European codes conservatively predict the ultimate strengths of the bolted connections, whereas the strengths predicted by the AS/NZS and SEI/ASCE specifications are overall more accurate and less scattered.

Keywords: Stainless steel; Bolted connections; Net section failure; Bearing failure; Block tearing failure; Finite Element Modelling; Design.

List of symbols

A gross cross-section area of the bolt

A_b nominal unthreaded body area of the bolt

A_e effective net area of the plate perpendicular to the direction of the load transfer

A_g gross area of the plate perpendicular to the direction of the load transfer

A_{net} or A_n net cross-section of the plate minus bolt holes, in a direction perpendicular to the applied force

A_{nt} net tension area of the plate

A_{nv} net shear area of the plate

A_s tensile stress area for bolts

$B_{p,Rd}$ the design punching shear resistance of the plate

E_0 elastic modulus

$F_{b,Rd}$ the design bearing resistance per bolt

$F_{NS,ult}$ ultimate load of net cross-section

$F_{NS,EC3}$ ultimate load predicted by Eurocode 3

$F_{NS,AISC}$ ultimate load predicted by AISC

F_t nominal tension stress for connections with washers under both bolt head and nut

$F_{t,Rd}$ the design tension resistance per bolt

F_u tensile strength of the connected material (AISC)

$F_{v,Rd}$ the design shear resistance per bolt

F_y yield strength of the connected material (AISC)

L_c the parallel length of the reduced section of the piece

L_E finite element size

$L_{1,e}$ length of external connection plate

$L_{1,i}$ length of internal connection plate

$N_{u,Rd}$ the design net section resistance of the plate

P_u the predicted ultimate load from design codes

$P_{u,FE}$ the ultimate load from finite element analysis

R_{pf} Stress at 0.2% non-proportional elongation

R_m tensile strength of bolt

R_n failure load according to AISC:2016

U_{bs} factor for block shear rupture design (AISC)

V_{eff} the design block tearing resistance of the plate

d_m, d nominal diameter of the bolt d_c basic minor diameter of external thread

d_f basic pitch diameter of external thread

d_0 the hole diameter for a bolt

e_1 end distance from the centre of the bolt hole, measured in the direction of the load transfer

e_2 edge distance from the centre of the bolt hole, measured perpendicular to the direction of the load transfer

$f_{0.2,meas}$ measured 0.2% proof stress from tensile coupon tests

$f_{0.2,cert}$ 0.2% proof stress from mill certificate

f_y yield strength of the plate

f_u ultimate strength of the plate

$f_{u,meas}$ measured ultimate stress from tensile coupon test

$f_{u,cert}$ ultimate stress from mill certificate

f_{yb} yield strength of the bolt

f_{ub} ultimate strength of the bolt

f_{up} characteristic ultimate strength of the plate

k_r reduction factor for net section failure

k_t reduction factor for bearing failure

l_{loc} average necking zone length

l_0 initial gauge length

l_c clear distance between the edges of two adjacent bolt holes or between the edge of a bolt hole and the edge of the connected material

n the total number of bolts in the connection

p_1 the spacing between centres of bolt holes, measured in the direction of load transfer

p_2 the spacing between a line of bolts, measured perpendicular to the direction of the load transfer

s spacing of bolts perpendicular to line of stress; in case of single bolt, s is the width of connected part

t, t_p thickness of the plate

t_e thickness of external connection plate

t_i thickness of internal connection plate

α_b reduction factor for bearing resistance

α_L localization rate factor

α_v reduction factor for shear resistance

$\gamma_{Mi.}$ partial safety factor

Φ resistance factor

Ω safety factor

ε_u strain corresponding to the ultimate tensile strength

μ friction coefficient

v Poisson ratio

$\varepsilon_{u,cert}$ strain corresponding to the ultimate tensile strength, from mill certificate

$\varepsilon_{u,meas}$ strain corresponding to the ultimate tensile strength, from tensile coupon test

λ_s finite element size factor

λ_E finite element type factor

$\gamma_{M0} = 1.00$ safety factor

$\gamma_{M2} = 1.25$ safety factor

1 General introduction

1.1 Duplex Stainless Steel

Stainless steel is a steel alloy that contains chromium in the range 10.5% to 30% in mass [1]. Depending on the chemical composition, four families of stainless steel exist, of which three are used in structural applications: the ferritic, austenitic and austeno-ferritic (duplex) grades. Their physical, chemical and mechanical properties vary with the family. Each grade is however characterized by the same ability to form a self-repairing protective oxide film providing corrosion resistance and a higher chromium content increases that resistance. Unlike austenitic grades which were mainly used as cladding (inside or outside), duplex grades are more and more used in structures where corrosion resistance combined with strength are the key design criteria. Typical stress-strain curves for duplex grades follow a nonlinear path with gradual yielding and large strain hardening domain. Duplex presents a microstructure characterized by a balance of 50% ferrite and 50% austenite [1]. They share the

properties of both families, are mechanically stronger than either ferritic or austenitic types and are ordinarily characterized by high resistance to stress corrosion cracking [2]. In [3] and [4], recent examples of stainless steel bridges are presented and a comprehensive list of the bridges incorporating main structural elements made of duplex steel is provided. Three different duplex grades were found in this research paper: EN 1.4162, EN 1.4362, EN 1.4462. The present paper deals with grades EN 1.4162 and EN 1.4462.

1.2 Design of bolted connections

A brief comparison between the European EN 1993-1-4 [5] and American AISC:2016 [6] design guidelines is made in this section.

Eurocode 3 is based on limit state design working with Ultimate Limit States (ULS) and Serviceability Limit States (SLS), making use of different safety factors γ_{M0}, γ_{M1} and γ_{M2} for both limit states. Whereas the Load and Resistance Factor Design (LFRD) has replaced the Allowable Strength Design (ASD) in AISC:2016 [6], AS/NZS 4673 [7] and SEI/ASCE 8-02 [8]. The main difference between the two methods lies in different factors. LFRD uses the resistance factor ϕ whereas ASD uses the safety factor Ω. To find the design strength, ϕR_n, or the allowable strength, R_n/Ω, the following factors should be used, i.e., $\phi = 0.75$ for LRFD and $\Omega = 2.00$ for ASD. Both methods are still used in the AISC-guide and values for both factors are included in each formula.

1.2.1 Geometries and material characteristics for bolts

The definition of the hole diameter d_0 according to ISO 20273 [9] is quite similar as that given in AISC:2016 (see Table J3.3M [6]). The end and edge distance, respectively e_1 and e_2, for bolts given in Table 3.3 in EN 1993-1-8 [10], are however different from those proposed in AISC:2016 [6]. In the latter, the spacing is defined as the distance between two centres of bolt holes and the edge distance is the distance from the centre of a hole to the edge of a connected part in any direction and is limited to 12 times the thickness of the connected part t as well as ≤ 150 mm. The AISC-guide prescribes that the distance between two bolt holes (min. spacing) should not be less than 2.67 times the nominal diameter d of the fastener and the rules for the maximum spacing are dependent on the nature of the elements to which the fastener is connected. It should be noted that in EN 1993-1-3 [11] there is no maximum limit for the e_1 and e_2 if 0.75 mm $\leq t_p <$ 3.0 mm. For $t_p >$ 3.0 mm, the minimum requirements for the spacings p_1 and p_2 are $2.2d_0$ and $2.4d_0$ as shown in Table 3.3 of EN 1993-1-8 [10]. These two parameters should be not greater than $14t$ or 200 mm. In accordance with AS/NZS 4673 [7] and SEI/ASCE 8-02 [8], the minimum distance between centres of bolt holes should not be less than $3d$, whereas the distance from the centre of any standard hole to the end or other boundary of the connecting plate should not be less than $1.5d$. There are no specific rules depend on the plate thickness.

Another minor difference is that, for single lap joints, EN 1993-1-8 [10] recommends the use of washers under the bolt head and nut when there is only one row of bolts.

EN 1993-1-8 [10] gives the nominal values of yield and ultimate tensile strength for carbon steel bolts for the most common used bolt classes ranging from 4.6 to 10.9. It is different in AISC:2016 [6] which uses bolt groups based on existing bolts from ASTM [12]. Stainless steel bolts are covered in EN ISO

3506 [13], in which bolt and nut materials are classified by a letter, e.g., “D” for duplex, followed by a number (1, 2, 3, 4, 5, 6 or 8) which reflects the corrosion resistance, 1 for least durable. The common designations of duplex stainless steels used for bolts of each class, the strength level and the corresponding mechanical properties can be found in [13]. To calculate the resistance of a bolt, the basic ultimate strength f_{ub} should be taken as the specified minimum tensile strength R_{m} from [13].

1.2.2 Failure modes and design formulae

This section briefly summarized the formulae from EN 1993-1-8 [10] and AISC:2016 [6] for four failure modes relevant to this paper.

1.2.2.1 Net cross-section failure

Failure of the plate occurs when excessive tension is transmitted by the bolts. The Design Manual For Structural Stainless Steel [14] prescribes the following formula for net cross-section failure**,** equ. (1):

$$\boldsymbol{N_{u,Rd} = A_{net} f_u / \gamma_{M2}} \quad (1)$$

Whereas, according to EN 1993-1-8 [10], the design ultimate resistance of the net cross-section at holes for fasteners should be determined as follows:

$$\boldsymbol{N_{u,Rd} = 0.9 A_{net} f_u / \gamma_{M2}} \quad (2)$$

And EN 1993-1-3 [11] prescribes the following formula for net cross-section failure:

$$\boldsymbol{F_{n,Rd} = \left(1 + 3r(d_0/u - 0,3)\right) A_{net} f_u / \gamma_{M2}} \quad (3)$$

With r being the number of bolts at the cross-section divided by the total number of bolts in the connection and $u = \min\{2e_2; p_2\}$.

The nominal values for tensile rupture strength can be found by the following equ. (4) according to AISC:2016 [6].

$$\boldsymbol{R_n = F_u A_e} \quad (4)$$

With A_e, the effective net area of the plate in a direction perpendicular to the applied force, limited to:

$$\boldsymbol{A_e \leq 0,85 A_g} \quad (5)$$

AS/NZS 4673 [7] and SEI/ASCE 8-02 [8] state the following equ. (6) to determine the nominal tensile capacity of the connected part P_n:

$$\boldsymbol{P_n = A_n F_t} \quad (6)$$

Where F_t is either $\boldsymbol{F_t = (1 - r + 2.5rd/s) F_u \leq F_u}$ for single shear connections or $\boldsymbol{F_t = (1 - 0.9r + 3.0rd/s) F_u \leq F_u}$ for double shear connections.

With r being the force transmitted by bolts at the considered section, divided by tension force in member at that section; if r is less than 0.2, it may be taken equal to zero.

In addition, the nominal tensile capacity of the connected part P_n should also be determined as follows:

$$\boldsymbol{P_n = A_n F_y} \quad (7)$$

1.2.2.2 Bearing failure of the plate

Bearing failure occurs when excessive pressure is applied by the bolt shaft on the plate. In [14], the following design formula for bearing resistance, equ. (8), is provided.

$$\boldsymbol{F_{b,Rd} = 2.5\alpha_b k_t f_u d t_p / \gamma_{M2}} \quad (8)$$

Two parameters, α_b and k_t, depend on the use of thick or thin plates ($t_p \leq 4$ mm). For the latter if the deformation is not the design criterion, we have:

Inner sheets in double shear connections: $\alpha_b = \min\{1.0; \frac{e_1}{3d_0}\}$ and $k_t = \begin{cases} 1.0 & for\ \frac{e_2}{d_0} > 1.5 \\ 0.8 & for\ \frac{e_2}{d_0} \leq 1.5 \end{cases}$.

Outer sheets in double shear connections: $\alpha_b = \min\{1.0; \frac{e_1}{2d_0}\}$ and $k_t = 0.64$.

If, however, the deformation is the design criterion, we have $\alpha_b = \min\{1.0; \frac{e_1}{2d_0}\}$ and $k_t = 0.5$.

According to EN 1993-1-8 [10], the bearing resistance should be determined as follows:

$$\boldsymbol{F_{b,Rd} = k_1 \alpha_b f_u d t_p / \gamma_{M2}} \quad (9)$$

$With\ \alpha_b = \min\{\alpha_d; \frac{f_{ub}}{f_u}; 1.0\}$. In the direction of load transfer, for end bolts, the recommendation is $\alpha_d = e_1/3d_0$ while it is $\alpha_d = p_1/3d_0 - 1/4$ for inner bolts. However, perpendicular to the direction of load transfer, it will be $k_1 = \min\{2.8e_2/d_0 - 1.7; 2.5\}$ or $k_1 = \min\{1.4p_2/d_0 - 1.7; 2.5\}$ for edge bolts and inner bolts respectively.

EN 1993-1-8 [10] gives, for single lap joints with one bolt row, the following limit, equ. (10), for each bolt.

$$\boldsymbol{F_{b,Rd} = 1.5 f_u d t_p / \gamma_{M2}} \quad (10)$$

Whereas, in accordance with EN 1993-1-3 [11], the bearing resistance should be determined as follows:

$$\boldsymbol{F_{b,Rd} = 2.5\alpha_b k_t f_u d t_p / \gamma_{M2}} \quad (11)$$

Where $\alpha_b = \min\{1.0; \frac{e_1}{3d}\}$, $k_t = (0.8t + 1.5)/2.5$ for $0.75\,mm \leq t_p \leq 1.25\,mm$ and $k_t = 1.0$ for $t_p > 1.25\,mm$.

According to AISC:2016 [6], the nominal bearing strength R_n of the connected plate at the bolt holes is given by equ. (12)**.**

$$\boldsymbol{R_n = 1.2 l_c t F_u \leq 2.4 d t F_u} \quad (12)$$

Equ. (12) only applies to standard, oversized and short-slotted bolt holes and in situations where the deformation at the bolt hole in service is a design consideration. When multiple bolts are present, the total bearing strength is equal to R_n times the number of bolts.

Last, in accordance with AS/NZS 4673 [7] and SEI/ASCE 8-02 [8], the bearing capacity per bolt of connected part, where we washers under both the bolt head and nut, is as follows:

For single shear connections: $\boldsymbol{P_n = 2 d t F_u}$ (13)

For double shear connections: $\boldsymbol{P_n = 2.75dtF_u}$ (14)

1.2.2.3 Tear out failure

According to AS/NZS 4673 [7] and SEI/ASCE 8-02 [8], tear out capacity of the connected part along two parallel lines in the direction of applied force shall be determined as follows:

$$\boldsymbol{P_n = teF_u} \quad (15)$$

With *e* being the distance measured in line of force from centre of standard hole to nearest edge of adjacent hole or to end of connected part and t the thickness of thinnest connected part.

1.2.2.4 Block tearing failure

Shear failure (in the direction parallel to loading) combined with tension failure (in the direction perpendicular to loading) is also known as block tearing failure. According to EN 1993-1-8 [10] the block tearing resistance for a symmetric bolt group subjected to a concentric load, $V_{eff,1,Rd}$, is given by equ. (16)**.**

$$\boldsymbol{V_{eff,1,Rd} = f_u A_{nt}/\gamma_{M2} + f_y A_{nv}/\sqrt{3}\gamma_{M0}} \quad (16)$$

According to AISC:2016 [6] however, the formula to find the block shear rupture strength of the material is equ. (17)**.**

$$\boldsymbol{R_n = 0.6F_u A_{nv} + U_{bs}F_u A_{nt} \leq 0.6F_y A_{gv} + U_{bs}F_u A_{nt}} \quad (17)$$

With $U_{bs} = 1$ when the tension stress is uniform (if not $U_{bs} = 0.5$).

The method to calculate values for A_{nv}, A_{nt} and A_{gv} is given in [6] and slightly differ from [10].

It should be noted that none of the European or North American standards explicitly formulate design expressions for block tearing resistance of connections with staggered bolt rows.

1.3 Current research

Experimental and numerical investigations on stainless steel bolted connections have been conducted by researchers worldwide. These are discussed and summarized in this section.

Salih *et al*. [15] numerically studied the net section failure in ferritic (grade 1.4016) and austenitic (grade 1.4306) stainless steel bolted connection. The performed parametric studies examined the effects of plate thickness, edge distance, bolt group configuration on the net section capacity of lap connections. It is suggested to directly use the ultimate material tensile strength without including a reduction factor in the design formula, which was generally found to greatly improve the design accuracy. The bearing failure of ferritic (grade 1.4016) and austenitic (grade 1.4306) stainless steel bolted connection was numerically investigated by Salih *et al.* [16]. Failure criterion was proposed on the basis of both strength and deformation concerns. The parametric studies were performed on both thick and thin sheet connections. Other investigated parameters included the end distances in the load direction and perpendicular to the load direction, connection type (i.e., single or double shear connections) and bolt group configuration. The improved bearing coefficients for both thin and thick sheet connections on the basis of both strength and deformation criterions were proposed.

According to EN 1993-1-8 [10], the resistance against net section failure is lowered by a reduction factor k_r, but Salih *et al.* [15] proved that this was in fact unnecessary. This was done by studying the effect of the bolt ratio r and edge distance ratio e_2/d_0 on multiple double shear bolted connections. Out of these numerical investigations, it was made clear that r did not have a significant effect on the strain distribution at the net section at failure in stainless steel connections. So, the ultimate material tensile strength can be used without including a reduction factor [15]. Kiymaz [17] also conducted numerical investigation into the bearing behaviour of stainless steel connections. The accuracy of the codified design rules was assessed, indicating a high level of conservatism and scatter. Talja and Torkar [18] carried out lap shear tests on ferritic stainless steel bolted and screwed connections, to examine the bearing failure and net section tension failure of the connections made of ferritic stainless steels. Regarding the calculation of the net section resistance, the best design approaches are EN 1993-1-1 with k_r = 1.0 or EN 1993-1-4. If deformation is the design criterion, EN 1993-1-1 gives the best agreement with k_r = 0.9. Last, block tearing was examined, and it was concluded that EN 1993-1-8 gives safe results although, if the deformation is the design criterion, the same code should be used with an extra correction factor of 0.9.

Cai and Young [19] performed experimental studies on austenitic (grades 1.4301 and 1.4571) and lean duplex (grade 1.4162) stainless steel bolted connections. The test programme was carefully designed, enabling both bearing and net section tension failures to be examined. In addition, various bolt groups with different bolt arrangements and numbers were studied. The structural behaviour of stainless steel single and double shear bolted connections at elevated temperatures was also studied by Cai and Young [20],[21]. The experimental study was performed by using steady state test method in the temperature ranged from 200 to 950 degrees. Comparisons of the test results against the predicted strengths by the SEI/ASCE-8 [8] and European codes [5],[10] generally indicate a high level of conservatism of the codified design rules for the bearing resistances of stainless steel connection at elevated temperatures. Improved bearing factors of stainless steel bolted connections at elevated temperatures were proposed by Cai and Young [22],[23], and were found to yield accurate and consistent bearing strength predictions. The transient state tests of cold-formed austenitic (grades 1.4301 and 1.4571) and lean duplex (grade 1.4162) stainless steel single shear and double shear bolted connections were also carried out by Cai and Young [21],[24]. Three different load levels of 0.25, 0.50 and 0.75 of the failure loads at room temperature were adopted in the transient state tests. A comprehensive comparison of the test results with those derived from the steady state tests were presented.

Kim and Lim [25] also investigated block tearing and the effect or curling. It was found that curling reduced the strength of the 2x1 array bolt connections against block tearing by minimum 11% and up to 26%. The issue Kim and Lim [25] addressed was that the current design standards do not consider the strength drop due to curling thus overestimating the strength.

Bouchaïr *et al*. [26] studied the structural behaviour of two different types of stainless steel connections, namely plate connections and T-stubs, where the bolts are loaded in shear and in tension, respectively. T-stub connections were used because they are mainly loaded in bending and shear leading to tension in the upper or lower bolts (depending on the direction of the bending moment).

The corresponding design rules were reviewed, and numerical models were developed and validated in the paper. Song *et al*. [27] conducted a series of tests of austenitic stainless steel bolts (A4-70 and A4-80) subjected to combined tension and shear. Based on their test results, a fracture model for stainless steel bolts was proposed, which could be applied in the simulation of stainless steel bolts in beam-to-column connections. Yuan *et al*. [28] tested stainless steel bolted T-stubs with various geometric configurations subjected to monotonic loading. Their investigations indicated that the design predictions from EN 1993-1-8 [10], AISC [6] and Chinese Code [29] were generally conservative. In [30], a new design equation for T-stub resistance based on the 3% proof strength is proposed, which better fits the experimental and numerical results.

No research was found regarding punching shear failure.

Table 1 summarizes the state of the art on tests and numerical studies related to stainless steel bolted connections, where it is clearly visible that the bulk of research on bolted connections was done on austenitic grades rather than on duplex ones. Hence, the main focus of this study is to investigate the behaviour of duplex stainless steel bolted connections, where the effects due to the spacings e_1, e_2, p_1 and p_2 as well as the bolt diameter and plate thickness are comprehensively studied. In addition, the current codified design rules for steel bolted connections are examined.

Table 1 Summary of recent research into stainless steel bolted connections

	Ferritic Stainless Steel			Austenitic Stainless Steel			Duplex Stainless Steel		
	Experiments	**Numerical work**	**Used codes**	**Experiments**	**Numerical work**	**Used codes**	**Experiments**	**Numerical work**	**Used codes**
Bearing failure of the plate	**[18] Single** - Grade: 1.4509 - Bolt: 12 - t: 0.5-4.5	**[16] Double** - Grade: 1.4016 - Bolt: 12,16,20 - t: 8	**[16] Double** - EN 1993-1-1,3&4	**[19] Single** - Grade: 1.4301/1.4571 - Bolt: 6;8;10;12 - t: 1.5	**[16] Double** - Grade: 1.4306 - Bolt: 12,16,20 - t: 10	**[16] Double** - EN 1993-1-1,3&4	**[19] Single** - Grade: 1.4162 - Bolt: 6;8;10;12 - t: 1.5	**[17] Single** - Grade: 1.4462 - Bolt: 25 - t: 13,5	**[17] Single** - EN 1993-1-1,3&4 - SEI/ASCE-8
		[16] Single - Grade: 1.4016 - Bolt: 20 - t: 1;2	**[16] Single** - EN 1993-1-1,3&4 - SEI/ASCE-8 - AS/NZS 4673	**[19] Double** - Grade: 1.4301/1.4571 - Bolt: 6;8;12 - t: 1.5	**[16] Single** - Grade: 1.4306 - Bolt: 20 - t: 1;2	**[16] Single** - EN 1993-1-1,3&4 - SEI/ASCE-8 - AS/NZS 4673	**[19] Double** - Grade: 1.4162 - Bolt: 6;8;12 - t: 1.5	**[22] Double** - Grade: 1.4162 - Bolt: 18;20;24 - t: 1.5;3.0;4.5	**[19] Single** - EN 1993-1-4 - SEI/ASCE-8 - AS/NZS 4673
		[16] Double - Grade: 1.4016 - Bolt: 20 - t: 1;2;8;10	**[16] Double** - EN 1993-1-1,3&4 - SEI/ASCE-8 - AS/NZS 4673	**[20] Single** - Grade: 1.4301/1.4571 - Bolt: 6;8;12 - t: 1.5	**[16] Double** - Grade: 1.4306 - Bolt: 20 - t: 1;2;8;10	**[16] Double** - EN 1993-1-1,3&4 - SEI/ASCE-8 - AS/NZS 4673	**[20] Single** - Grade: 1.4162 - Bolt: 8;12 - t: 1.5	**[23] Single** - Grade: 1.4162 - Bolt: 18;20;24 - t: 1.5;3.0;4.5	**[19] Double** - EN 1993-1-4 - SEI/ASCE-8 - AS/NZS 4673
			[18] Single - EN 1993-1-1,3,4&8	**[21] Double** - Grade: 1.4301/1.4571 - Bolt: 6;8;12 - t: 1.5	**[17] Single** - Grade: 1.4301 - Bolt: 25 - t: 13,5	**[17] Single** - EN 1993-1-1,3&4 - SEI/ASCE-8	**[21] Double** - Grade: 1.4162 - Bolt: 8;12 - t: 1.5		**[20] Single** - EN 1993-1-4 - SEI/ASCE-8 - AS/NZS 4673

		[24] Single - Grade: 1.4301/1.4571 - Bolt: 6;8;12 - t: 1.5	**[22] Double** - Grade: 1.4301/1.4571 - Bolt: 18;20;24 - t: 1.5;3.0;4.5	**[19] Single** - EN 1993-1-4 - SEI/ASCE-8 - AS/NZS 4673	**[24] Single** - Grade: 1.4162 - Bolt: 8;12 - t: 1.5	**[21] Double** - EN 1993-1-4 - SEI/ASCE-8 - AS/NZS 4673
			[23] Single - Grade: 1.4301/1.4571 - Bolt: 18;20;24 - t: 1.5;3.0;4.5	**[19] Double** - EN 1993-1-4 - SEI/ASCE-8 - AS/NZS 4673		**[22] Double** - EN 1993-1-4 - SEI/ASCE-8 - AS/NZS 4673
				[20] Single - EN 1993-1-4 - SEI/ASCE-8 - AS/NZS 4673		**[23] Single** - EN 1993-1-4 - SEI/ASCE-8 - AS/NZS 4673
				[21] Double - EN 1993-1-4 - SEI/ASCE-8 - AS/NZS 4673		
				[22] Double - EN 1993-1-4 - SEI/ASCE-8		

						- AS/NZS 4673			
						[23] Single - EN 1993-1-4 - SEI/ASCE-8 - AS/NZS 4673			
Failure of net cross-section	**[18] Single** - Grade: 1.4509 - Bolt: 12 - t: 0.5-4.5	**[15] Double** - Grade: 1.4016 - Bolt: 12,16,20 - t: 8	**[15] Double** - EN 1993-1-1,3&4	**[19] Single** - Grade: 1.4301/1.4571 - Bolt: 6;8;10;12 - t: 1.5	**[15] Double** - Grade: 1.4306 - Bolt: 12,16,20 - t: 10	**[15] Double** - EN 1993-1-1,3&4	**[19] Single** - Grade: 1.4162 - Bolt: 6;8;10;12 - t: 1.5		**[19] Single** - EN 1993-1-4 - SEI/ASCE-8 - AS/NZS 4673
			[18] Single - EN 1993-1-1,3,4&8	**[19] Double** - Grade: 1.4301/1.4571 - Bolt: 6;8;12 - t: 1.5		**[19] Single** - EN 1993-1-4 - SEI/ASCE-8 - AS/NZS 4673	**[20] Single** - Grade: 1.4162 - Bolt: 8;12 - t: 1.5		**[20] Single** - EN 1993-1-4 - SEI/ASCE-8 - AS/NZS 4673
				[20] Single - Grade: 1.4301/1.4571 - Bolt: 6;8;12 - t: 1.5		**[19] Double** - EN 1993-1-4 - SEI/ASCE-8 - AS/NZS 4673	**[21] Double** - Grade: 1.4162 - Bolt: 8;12 - t: 1.5		**[21] Double** - EN 1993-1-4 - SEI/ASCE-8 - AS/NZS 4673
				[21] Double - Grade: 1.4301/1.4571		**[20] Single** - EN 1993-1-4	**[24] Single** - Grade: 1.4162		

				- Bolt: 6;8;12 - t: 1.5		- SEI/ASCE-8 - AS/NZS 4673	- Bolt: 8;12 - t: 1.5
				[24] Single - Grade: 1.4301/1.4571 - Bolt: 6;8;12 - t: 1.5		**[21] Double** - EN 1993-1-4 - SEI/ASCE-8 - AS/NZS 4673	
Block tearing	**[18] Single** - Grade: 1.4509 - Bolt: 12 - t: 0.5-4.5		**[18] Single** - EN 1993-1-1.3.4&8	**[25] Single** - Grade: AISI 490 - Bolt: 12 - t: 3	**[25] Single** - Grade: AISI 490 - Bolt: 12 - t: 3	**[25] Single** - SEI/ASCE-8 - AIJ (Japan) - AISC	
Tension failure of the bolt				**[26] T-stub** - Grade: 1.4306 - Bolt: 12;16		**[26] T-stub** - EN 1993-1-1.3&4	

2 Finite element model validation

The objective of this section is to demonstrate that our FEM can accurately represent the behaviour of duplex bolted connections. The net cross-section, bearing and combined bearing and net cross-section failure modes are investigated for a series of configurations as will be described. FE analyses were conducted using the research edition of the commercial ABAQUS/Explicit code [32].

It is worth noting that experiments on bolted connections are quite difficult to reproduce numerically. This can be noticed in almost all research papers presented in the literature survey in this paper, as for example, the load-displacement curves of the first and repeated tests reported in Cai and Young [19]. The most probable influencing parameters are here the bolt position in its hole as well as the possible load eccentricity. An additional complexity making tests of bolted connections difficult to reproduce numerically relates to the level of preload, i.e., all the plates being pulled into firm contact by the bolts in the joint, and the surface condition which affects the friction between the plates. In sum, the main difficulty relates to reproducing the initial part of the response and the stiffness, whilst the maximum load and the failure mode are more easily simulated.

2.1 Mesh and boundary conditions

2.1.1 Net cross-section failure

The first experiments used to validate our FEM included net cross-section failure of plates produced from duplex stainless steel grade 1.4462. The varying parameter in experiments was the edge distance e_2 (see Figure 1 and Table 2).

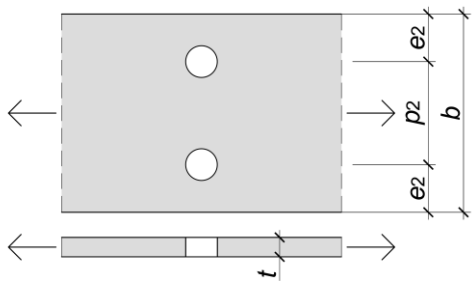

Figure 1 Front and plan view of a type 1 (S) connection

Table 2 Geometry of the duplex net cross-section test specimens

Model no.	Plate dimensions [mm]						Grade
	t	e_2	e_2/d_0	p_2	b	d_0	
SSD7	4	27	1.5	45	99	18	1.4462
SSD8	4	36	2.0	45	117	18	1.4462
SSD9	4	45	2.5	45	135	18	1.4462

Stereo vision Digital Image Correlation (DIC) was used to identify the displacement field during the tests. This optical measurement technique uses two cameras to triangulate each subset of a speckle pattern usually painted onto the measured surface and to generate a full 3D point cloud of the pattern.

The comparison of subsequent patterns during the test allows to compute a deformed surface. The tests load speed was 2.5 kN/min. Synchronized pictures were taken at 0.1 Hz to follow the displacements. They were used for the correlation of the point cloud in the software MatchID [31]. The force-average displacement curve for SSD7, SSD8 and SSD9 are given in Figure 2.

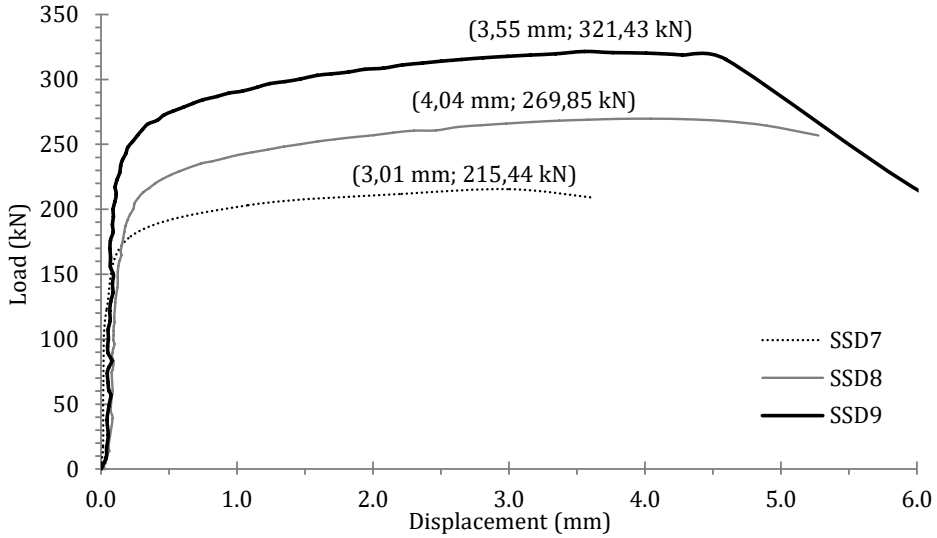

Figure 2 Force-Displacement diagram for SSD7, SSD8 and SSD9

Specimens SSD7 and SSD8 showed a net cross-section failure that went from necking from the edges to complete net section failure. From here, strength dropped slightly while plastic deformation continued causing failure eventually. Unlike the previous test, SSD9's (e_2 = 45 mm) failure mode was slightly different. Even though the previous phenomena, necking and eventually net section failure, also occurred, in between those events the mid-section between the bolt holes prematurely ruptured (at an ultimate strength of 321.43 kN and a displacement of 3.55 mm). Due to this partial fracture, the force in the curve lowers slightly though deformation keeps growing. Next, cracks initiated at the sides of the bolt holes, until complete net section failure. Figure 11 illustrates the principal (logarithmic) strains around the bolt holes for SSD9 obtained using DIC around the failure load at 4 different representative moments. Figure 3 depicts the mesh used in the FEM of these experiments with the mesh refinement around the bolt hole.

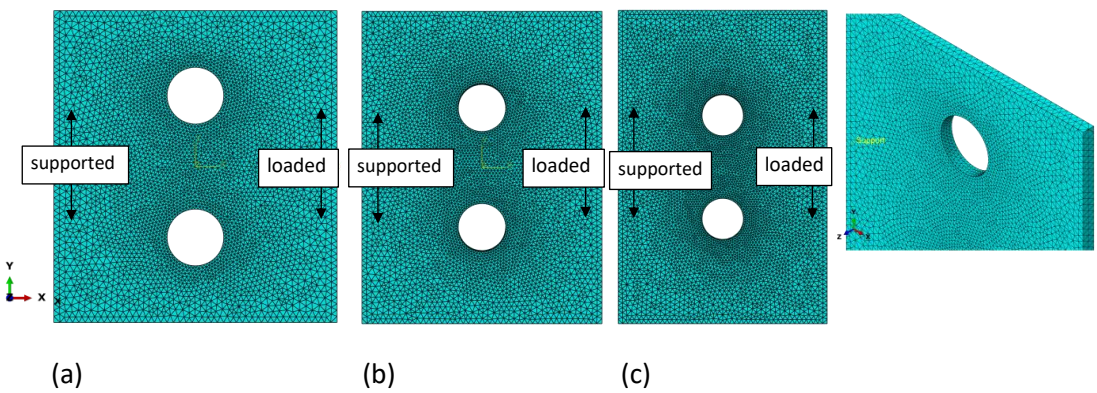

Figure 3 Components and mesh for (a) SSD7, (b) SSD8 and (c) SSD9

2.1.2 Single and double shear bolted connections

In [19], bearing and combined bearing and net cross-section failure modes are described for single and double shear connections with lips, as seen in Figure 4. Lips with normal height of 10 mm were designed in these connection plates in order to prevent the out-of-plane curling at the overlapped connection region. In this paper, the tests labelled L-S-1-12, L-D-1-12, L-D-2Pa-8-r, L-D-2Pe-8 and L-S-3-8 are used as basis to validate the FE model. In particular, in this section, double shear connection, namely L-D-2Pa-8, will be used to calibrate FE parameters as is described here below.

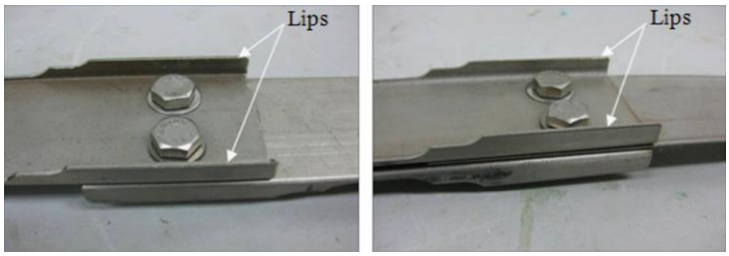

Figure 4 Single and double shear double-bolted connection, adapted from [19]

The geometry and boundary conditions of the FE model including details of the connection, are shown in Figure 5. The geometry of all the presented FE models is based on the measured dimensions of the specimens. The dimensions of the bolt, including the threaded portion, are taken from ISO 262 [33], the pitch is 1.75 mm and pitch angle is 60°. The FE mesh of the plates, bolts, nuts and washers is made using the finite tetrahedron solid element named C3D4. A global element size of 2 mm is used for all plates with at least two elements through the thickness in order to properly take into account the bending stiffness. The mesh density is increased in regions around the holes and the FE dimension in the regions where fracture is expected is set to be 0.6 mm. In addition, the FE dimension of the bolts, nuts and washers is set to 1 mm in order to gain accuracy in the complex geometry of the threads. Mesh refinement was studied for all models until acceptable convergence was reached. For the element size of the connected plates, a mesh sensitivity study was performed with sizes 5 mm, 2 mm and 1 mm. A size of 2 mm was chosen provided that almost the same results as those with 1 mm were obtained at much less computation costs.

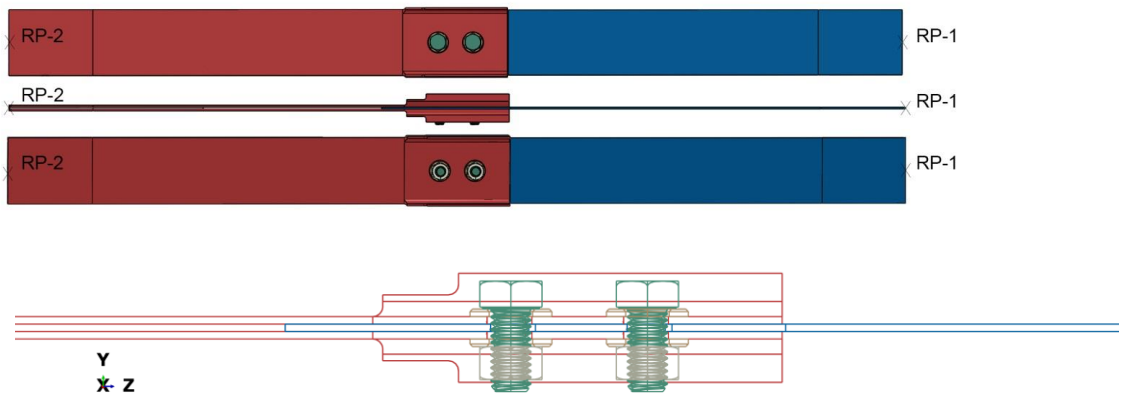

(a)

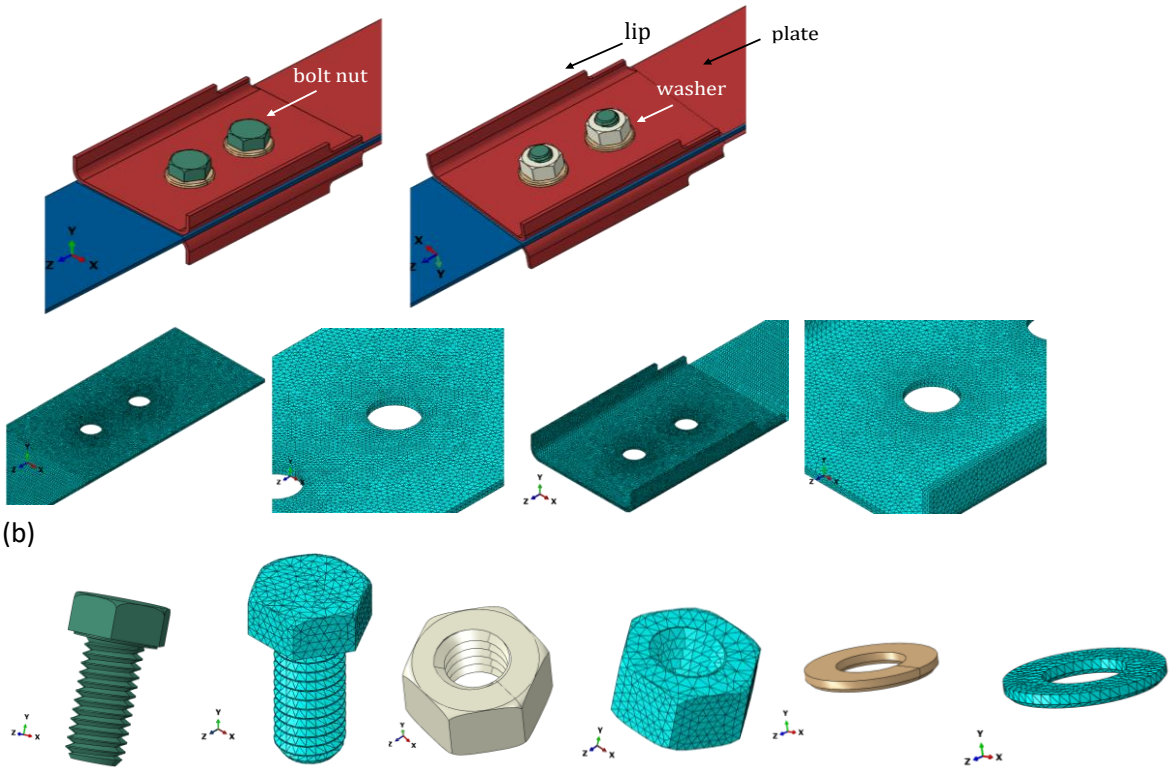

Figure 5 Components and typical mesh in FE models of connections from [19]: (a) typical double shear lap connection (whole connection and cross-section), (b) components included in a double shear lap connection, (c) focus on bolt, washer and nut, (d) boundary conditions – top and bottom end of double shear connection

In the case of shear connections, nodes of external surfaces at the top connection's end were kinematical constrained to a reference point RP-2 named "Jack". Displacement controlled failure loading was defined to this reference point, enabling the post-ultimate behaviour in the nonlinear analysis to be captured. Nodes of the external surfaces at the bottom connection's end were kinematical constrained to the reference point RP-1 named "Support" where the total reaction force RF3 was calculated. Both reference points were placed at the centroids of the connection's end cross-sections. The length of the end external surfaces coupled with the reference points is equal to 65 mm, considering that the tested connections were gripped in the gripping apparatus with a constant length of 65 mm [19]. The degrees of freedom set in the reference points correspond to the boundary conditions of the experiment: each end of the specimen was joined by a gripping apparatus which was free to rotate in one direction through pin-ends; one end of the connection plate was fixed while the other end was free to move [19]. In the case of double shear bolted connection specimens, the additional internal plate with 150 mm length, having the same thickness as the middle plate of the

connection specimens, is modelled to allow concentric load application. In all numerical simulations, it is assumed that all specimens are concentrically loaded, i.e., the possible connection eccentricity and moment effects are ignored. Besides, both plates in single shear connections and both external plates and internal plate in double shear connections are also moved in opposite directions to eliminate a uniform clearance of 0.3 mm between the bolt shank and the bolt hole, and to prevent large bolt slippage in the numerical simulations, as in [19]. Note that the numerical simulations of experiments do not account for initial geometric imperfections of both the connected plates and the bolts.

2.2 Time increment

At this point, it is worth noting that the FE analyses were performed as quasi-static with dynamic explicit solver. However, the application of explicit dynamics to analyse quasi-static problems leads to impractical computational time cost. In order to obtain economic quasi-static solutions, the calculation speed may be increased by using time scaling or mass scaling techniques. However, these methods tend to increase inertia forces in a model, sometimes leading to useless results. Hence, the process should be modelled in an acceptable time frame in which the dynamic effects would be insignificant and deviations of the obtained results in comparison with the static solution would not be considerable. The mass scaling technique is based on the principle that artificially increases the density of a numerical model to encourage minimal stable time increments. However, higher densities might induce higher kinetic energy. And it can be considered that the quasi-static solution is achieved if the ratio of the kinetic energy and internal energy in the numerical model is lower than 10% [34]. Mass scaling with desired time increment of 0.0001 was presently used for all numerical models. Scaling was set to be variable (recomputed in every integration step) and non-uniform (different for each FEM) as it is the most efficient for those models including large spectra of elements sizes and damage.

To achieve the quasi-static solution and to identify the applicable mass scaling value for numerical analyses, the kinetic energy-to-internal energy ratio was examined through a sensitivity study of structural response of double shear connection L-D-2Pa-8. Figure 6a shows, in a diagrammatic form, the results of a sensitivity study performed on the different target time increment values applied in explicit integration procedures, involving values of 0.0005, 0.0001 and 0.00008. It may be observed in this figure that the value of 0.0001 produces reliable numerical results as the kinetic energy after 80 s is smaller than 7% of the total internal energy. In addition, the quality of the results was verified by matching the input and output forces in a model for displacement-controlled failure loading, as it is shown in Figure 6b. Linear matching curve, which corresponds to the time increment value of 0.0001, with no oscillations proves that no inertia effects govern the results. The same matching curves for larger time increments (0.01 and 0.001) are also shown in this figure for comparison purposes.

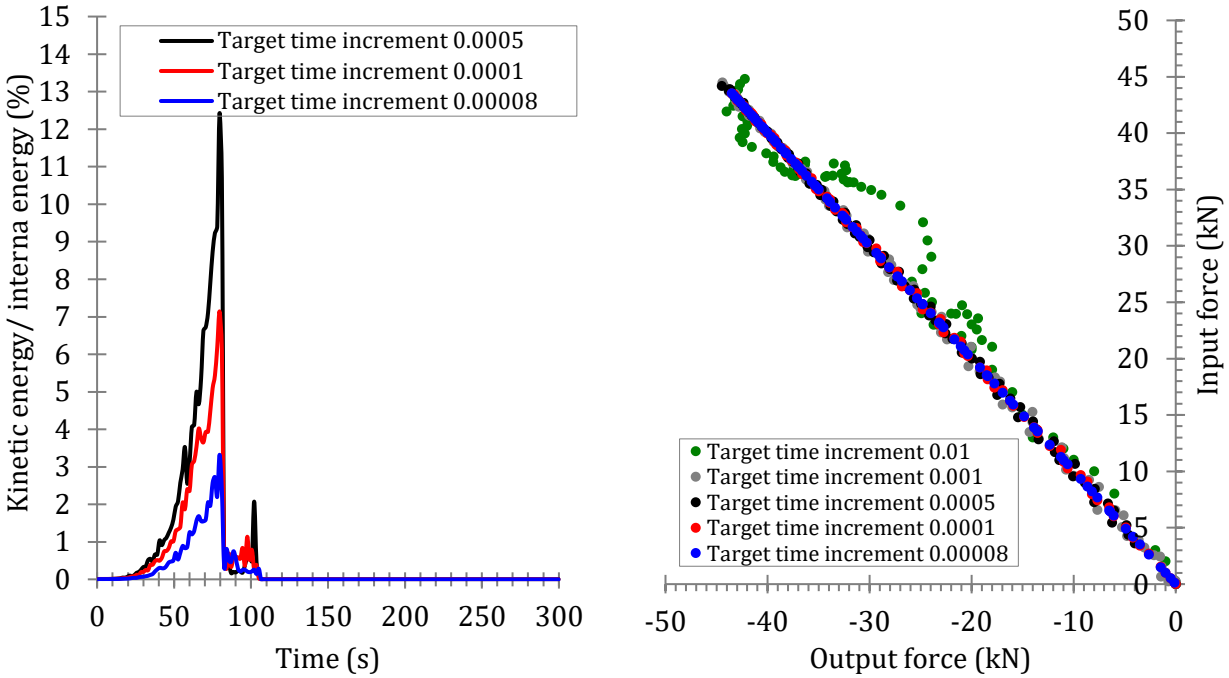

(a) Kinetic energy-to-internal energy ratio vs. time period

(b) Input force vs. output force

Figure 6 Quality of quasi-static solution using mass scaling technique.

2.3 Material model and contact conditions

The stress-strain curve and tensile fracture behaviour of duplex stainless steel plates at ambient temperature condition were investigated. The test results were used for the validation of the fracture simulation in the finite element (FE) model. The ambient temperature material properties of duplex 1.4462 were firstly tested through tensile coupon tests. The coupons were cut out in the transverse direction (perpendicular to the rolling direction of the plate). Based on the thicknesses used in the test specimens, the geometry for all dog-bone coupons were calculated and the coupons were cut accordingly. The cross-sections were measured with a digital calliper with a precision of 0.01 mm. To test the coupons, an electromechanical tensile testing machine was used, model INSTRON 5900, with a maximum tensile force of 100 kN. An extensometer model INSTRON 2630-100 Series Clip-on was used to measure the elongation. With a range from -5 mm up to 50 mm, it can measure bi-directional displacements. The accuracy of this measuring device ranges around 0.5%. Tests were based on strain rate control according to with ISO standard 6892-1 [35]. Based on tensile coupon tests, the material properties of both the 3 mm and 4 mm duplex 1.4462 grade plates (obtained from Outokumpu) were determined in accordance with ISO standard 6892-1 [35] annex D, see Table 3. In Table 3, the important mill certificate mechanical properties in the transverse direction (at a room temperature between 20 and 25 °C) are also listed, for comparison. It shows that the transversal ductility is usually lower than the longitudinal one.

Table 3 Results of tensile tests in comparison with mill certificate ones

		$f_{0.2,meas}$ [MPa]	$f_{0.2,cert}$ [MPa]	$f_{u,meas}$ [MPa]	$f_{u,cert}$ [MPa]	$\varepsilon_{u,meas}$ [%]	$\varepsilon_{u,cert}$ [%]	$f_{0.2,meas}$ / $f_{0.2,,cert}$	$f_{u,meas}$ / $f_{u,cert}$	$\varepsilon_{u,meas}$ / $\varepsilon_{u,cert}$
3 mm	C1	510.93	650	798.86	823	-	34	0.79	0.97	-
	C2	642.44		777.54		-		0.99	0.94	-
	C3	667.25		786.47		31.12		1.03	0.96	0.92
4 mm	C1	557.71	644	808.04	853	33.40	32	0.87	0.95	1.04
	C2	584.26		797.72		31.50		0.91	0.94	0.98
	C3	642.61		797.48		-		1.00	0.93	-

In the FE models, material, geometrical and contact nonlinearities were incorporated using the PLASTIC, NLGEOM and CONTACT PAIR commands respectively in ABAQUS. The general contact interaction procedure is chosen in the FE software package with a hard formulation in the normal direction and penalty friction formulation in the tangential one to enforce frictional resistance and no-sliding behaviour. A friction coefficient of 0.14 is chosen for the bolts and nuts threaded surface pairs in all FE models. For all other contact pairs in the models, the friction coefficient is ranging between 0.0 (frictionless) and 0.20. The surfaces that are anticipated to interact with each other in the FE models include the bolt shank to bolt holes, bolt thread to nut thread, the washers to plates and the internal plates to external plates.

The measured stress-strain curves are used for the material of the plates in order to validate the FE model. In the absence of measured data, such as for the bolts, washers and nuts, the nominal values of the yield and ultimate stresses are used, with the elongation at fracture A = 0.3d mm for bolt material grade A4-80 according to ISO 3506-1 [13]. The modified Ramberg-Osgood analytical model [36] is employed to model the nonlinear material response up to the ultimate tensile strength. Engineering stress-strain curves are transformed to the true stress-strain curves to be inputted in the ABAQUS plasticity model.

Table 4 provides the material parameters included in the FE models for the flats and corners of the studied cross-sections: the yield strength f_y taken as the 0.2 % proof strength, the ultimate tensile strength f_u, the strain corresponding to the ultimate tensile strength ε_u, and the strain hardening parameters n and m.

Table 4 Key material properties adopted in the FE models

Stainless steel grade	f_y (N/mm^2)	f_u (N/mm^2)	ε_u (%)	Strain hardening parameters	
				n	m
EN 1.4162	675	813	36.8	4	3.3
EN 1.4462	558	808	33.4	7	2.9
A4-80	251	703	57.0	7	3.1

The stress–strain curves used in FE material modelling are presented in Figure 7a. Isotropic plasticity with an initial modulus of elasticity of E_0 = 200 GPa and Poisson's ratio of v = 0.3 is used for all the materials. The ductile damage model is used for the plates, in order to account for element removal and accurately model the failure mode. The hardening part of the material behaviour is therefore

defined by the nonlinear plasticity curve while the softening part and failure are governed by the damage initiation criterion and the damage evolution law, as described in the next section.

2.3.1 Damage model

Parameters for the ductile damage initiation criterions are assessed by using an engineering approach as per [37], [38] that process the raw experimental data of the standard tensile tests in the *i*-th phase of the loading sequence and implements the principles of progressive damage model described in ABAQUS [32]. The flat tensile coupons for both duplex grades EN 1.4462 and EN 1.4162 were numerically modelled, and the material parameters calibrated by comparing the numerical results to the corresponding experimental data. For each material model, three specific ranges were developed: undamaged constitutive behaviour (parts *p*-*n*-*r'*-*f'*), damage initiation criterion (point *n*) and damage evolution law (parts *n*-*r*-*f*), where *p* is the onset of plasticity, *n* is the onset of necking, *r* is the rupture point, and *f* is the fracture point. Figure 7a highlights these ranges in the curve for the flat coupon EN 1.4462.

First, the damage initiation criterion was defined as the equivalent plastic strain at the onset of damage $\overline{\varepsilon}_0^{\mathrm{pl}}$. The ductile criterion provided in [32] assumes that the equivalent plastic strain at the onset of damage $\overline{\varepsilon}_0^{\mathrm{pl}}$ is a function of the stress triaxiality ratio θ and the strain rate. In the case of uniaxial tension $\theta = 1/3$, and the equivalent plastic strain at the onset of damage can be defined as $\overline{\varepsilon}_0^{\mathrm{pl}} = \varepsilon_0^{\mathrm{pl}} = \varepsilon_{\mathrm{n}}^{\mathrm{pl}}$, where $\varepsilon_{\mathrm{n}}^{\mathrm{pl}}$ is the uniaxial true plastic strain at onset of necking that is determined using the experimental data of standard tensile tests.

Based on the experimental and theoretical findings of Trattnig et al. [39] and Rice and Tracey [40], Pavlović et al. [37] proposed an exponential dependency between the equivalent plastic strain at the onset of damage $\overline{\varepsilon}_0^{\mathrm{pl}}$ on the one hand, and the uniaxial true plastic strain at the onset of damage $\varepsilon_{\mathrm{n}}^{\mathrm{pl}}$ and triaxiality θ on the other hand:

$$\overline{\boldsymbol{\varepsilon}}_{\mathbf{0}}^{\mathbf{pl}}(\boldsymbol{\theta}) = \boldsymbol{\varepsilon}_{\boldsymbol{n}}^{\mathbf{pl}} \, \mathbf{exp}[\mathbf{-1.5}(\boldsymbol{\theta}\mathbf{-1/3})] \tag{18}$$

The damage initiation criterions according to equ. (18) are shown in Figure 7b.

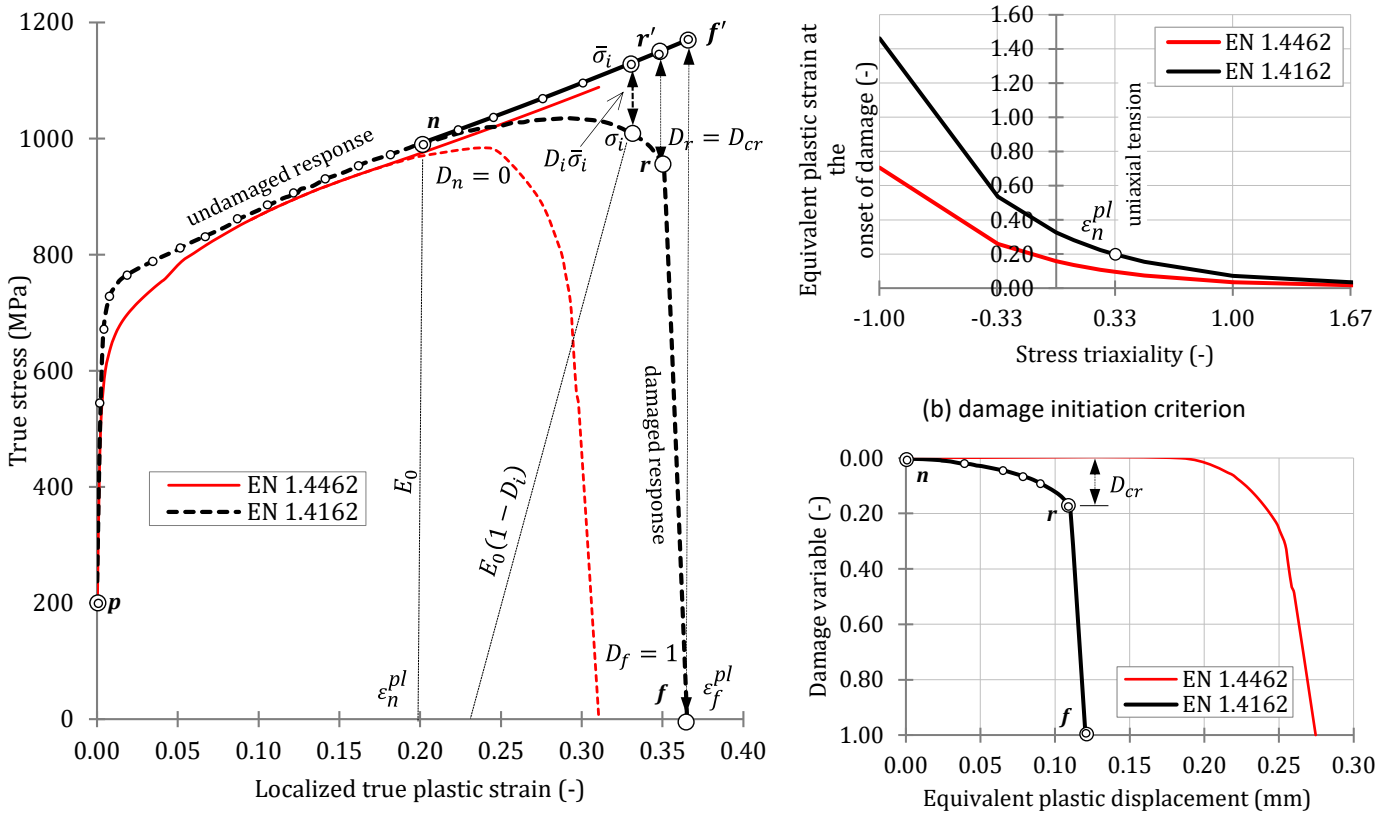

(a) plasticity curve

(b) damage initiation criterion

(c) damage evolution law

Figure 7 Plasticity and ductile damage parameters for flat coupons form stainless steel grades EN 1.4462 and EN 1.4162

The first part of the undamaged material response up to point *n*, was developed by converting the experimental stress–strain curve to the true stress–strain curve:

$$\boldsymbol{\varepsilon_i} = \ln(\mathbf{1} + \boldsymbol{\varepsilon_i^{nom}}) \tag{19}$$

$$\boldsymbol{\sigma_i} = \boldsymbol{\sigma_i^{nom}}(\mathbf{1} + \boldsymbol{\varepsilon_i^{nom}}) \tag{20}$$

where nominal strains ε_i^{nom} are given by the equ. (21).

$$\boldsymbol{\varepsilon_i^{nom}} = \boldsymbol{\Delta l_i / l_i}, \quad \boldsymbol{i < n} \tag{21}$$

The second part of the undamaged curve after the onset of necking (point *n*), was developed assuming a perfectly plastic material behaviour in accordance with equs. (22) and (23) :

$$\boldsymbol{\varepsilon_i^{pl}} \cong \ln(\mathbf{1} + \boldsymbol{\varepsilon_i^{nom}}) - \ln\left(\mathbf{1} + \boldsymbol{\varepsilon_p^{nom}}\right), \quad \boldsymbol{i \geq n} \tag{22}$$

$$\boldsymbol{\overline{\sigma}_i} = \boldsymbol{\sigma_n^{nom}}(\mathbf{1} + \boldsymbol{\varepsilon_i^{nom}}), \quad \boldsymbol{i \geq n} \tag{23}$$

The nominal strains ε_i^{nom} were obtained by equ. (24):

$$\boldsymbol{\varepsilon_i^{nom}} = \boldsymbol{\varepsilon_{i-1}^{nom}} + (\boldsymbol{\Delta l_i - \Delta l_{i-1}})/\boldsymbol{l_i}, \quad \boldsymbol{i \geq n} \tag{24}$$

In the aforementioned equs. (21) and (24), the variable gauge length l_i is defined by equ. (25) at every loading stage *i* as a function of elongation Δl_i:

$$\boldsymbol{l_i} = \begin{cases} \boldsymbol{l^0}, & \boldsymbol{i < n} \\ \boldsymbol{l^0 + \left(l^{loc} - l^0\right)[(\Delta l_i - \Delta l_n)/(\Delta l_r - \Delta l_n)]^{\alpha_L}}, & \boldsymbol{i \geq n} \end{cases} \quad (25)$$

where l^0 is the initial gauge length (25 mm and 55 mm for coupons from stainless steel grade EN 1.4162 and EN 1.4462, respectively), l^{loc} is the average length of the necking zone and α_L is the localization rate factor given in Table 5.

The damage evolution law defines the post damage-initiation material behaviour and describes the rate of degradation of the material stiffness in the region of strain localization once the damage initiation criterion is reached. The formulation is based on the Lemaitre damage model [41] that uses the scalar approach:

$$\overline{\boldsymbol{\sigma}} = \boldsymbol{\sigma}/(\mathbf{1} - \boldsymbol{D}) \quad (26)$$

where D is the damage variable adopted to describe the relationship between the undamaged and damaged material response, $\overline{\sigma}$ is the undamaged, effective stress that would exist in the material in the absence of damage, and σ is the true stress. At the point of material damage initiation *n* that corresponds to the onset of necking (point n), the damage variable is $D = 0$. At the point *r* the material undergoes a critical value of damage D_{cr} ranging between 0.2 and 0.8 depending on the material type [41]. At the fracture point *f* with a total degradation of the stiffness, the damage variable $D = 1$. The damage variable D_i is the dimensionless difference between the undamaged and damaged response of the material model, as follows:

$$\boldsymbol{D_i} = \begin{cases} \mathbf{1} - \boldsymbol{\sigma_i}/\overline{\boldsymbol{\sigma}}_{\boldsymbol{i}}, & \boldsymbol{n \leq i < r} \\ \mathbf{1}, & \boldsymbol{i = f} \end{cases} \quad (27)$$

The damage evolution laws were included in the FE material models in tabular form i.e., the damage variable D_i in function of the equivalent plastic displacement $\overline{u}_i^{pl}$ at the loading stage *i* after the onset of damage. Values of $\overline{u}_i^{pl}$ were obtained using the following equation:

$$\overline{\boldsymbol{u}}_{\boldsymbol{i}}^{\mathbf{pl}} = \overline{\boldsymbol{u}}_{\boldsymbol{f}}^{\mathbf{pl}}\left(\boldsymbol{\varepsilon}_{\boldsymbol{i}}^{\mathbf{pl}} - \boldsymbol{\varepsilon}_{\boldsymbol{n}}^{\mathbf{pl}}\right)/\left(\boldsymbol{\varepsilon}_{\boldsymbol{f}}^{\mathbf{pl}} - \boldsymbol{\varepsilon}_{\boldsymbol{n}}^{\mathbf{pl}}\right), \quad \boldsymbol{i \geq n} \quad (28)$$

Figure 7c illustrates the damage evolution laws.

The use of the stress-strain relationship in the FE model introduces a strong mesh dependency based on strain localization. Thus, the total equivalent plastic displacement at fracture $\overline{u}_f^{pl}$ can be determined by equ. (29)

$$\overline{\boldsymbol{u}}_{\boldsymbol{f}}^{\mathbf{pl}} = \boldsymbol{\lambda_S L_{char}}\left(\boldsymbol{\varepsilon}_{\boldsymbol{f}}^{\mathbf{pl}} - \boldsymbol{\varepsilon}_{\boldsymbol{n}}^{\mathbf{pl}}\right) \quad (29)$$

where λ_S is the factor of FE size, L_{char} is the characteristic element length and $\left(\varepsilon_f^{pl} - \varepsilon_n^{pl}\right)$ is the difference between the plastic strain at fracture ε_f^{pl} and at the onset of necking ε_n^{pl}.

The characteristic element length depends on the size and type of FE:

$$\boldsymbol{L_{char}} = \boldsymbol{\lambda_E L_E} \quad (30)$$

where L_E is the element size and λ_E is the element type factor.

The parameters for ductile damage calculation are evaluated through the calibration of the numerical data against the corresponding experimental data from the standard tensile tests. They are summarized in Table 5.

The applicability of the presented procedure to ductile material damage model has been confirmed in previous researches, both for conventional [42], [43], [44] and high strength carbon steel [45].

Table 5 Identified parameters for ductile damage calculation

Material	Damage	Element type		Element size		Localization	
	Initiation strain	Type	Factor	Size (mm)	Factor	Length (mm)	Factor
	ε_n^{pl}		λ_E	L_E	λ_s	l^{loc}	α_L
Coupon EN 1.4462	0.096	Solid C3D4	1.5	0.6	1.6	10	0.29
Coupon EN 1.4162	0.198	Solid C3D4	1.2	0.6	1.0	5	0.79

Figure 8 shows a comparison between the measured stress-strain relationship of the tensile test on coupon C1 and its counterpart gained from FEM. The same FE type as well as FE dimension set in the model of tensile coupon tests are used to model the plates involved in the connection simulations i.e., net section failure and shear bolted connection tests.

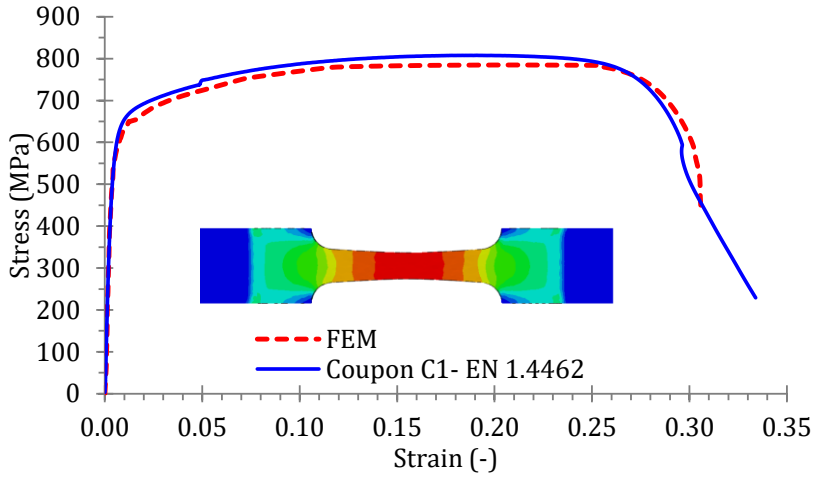

Figure 8 Comparison of engineering and FEM tensile test data for plates used in net section failure tests

2.4 FEM Validation

2.4.1 Net cross-section failure

The FE model for net cross-section failure is able to very accurately represent the final failure mode (necking and, in the case of SSD9, cracking between the bolts leading eventually to failure) as well as the force-displacement curves of all three experiments (see Figure 9). To illustrate the capability of the developed FE models for predicting the onset of failure and an approximation of the physical damage response, Figure 9 also depicts the numerical load-displacement curves based on the undamaged elastic-plastic material response. Slightly lower stiffness was obtained which could be attributed to a slightly higher Young's modulus for the duplex grade than the nominal one used in the FEM but this was however not proven during the experimental campaign. Figure 10 shows the Von Mises stress and

corresponding damage at failure for SSD7, SSD8 and SSD9. In addition, Figure 11 shows the principal logarithmic strain field at 4 moments before and after for SSD9. The experimental-to-numerical ultimate load ratios are 0.95, 1.01 and 1.00 for SSD7, SSD8 and SSD9 respectively. And the experimental-to-numerical displacement ratios corresponding to the ultimate loads $\delta_{u,FEM}/\delta_{u,test}$ are 0.85, 1.10 and 0.94 for SSD7, SSD8 and SSD9 respectively.

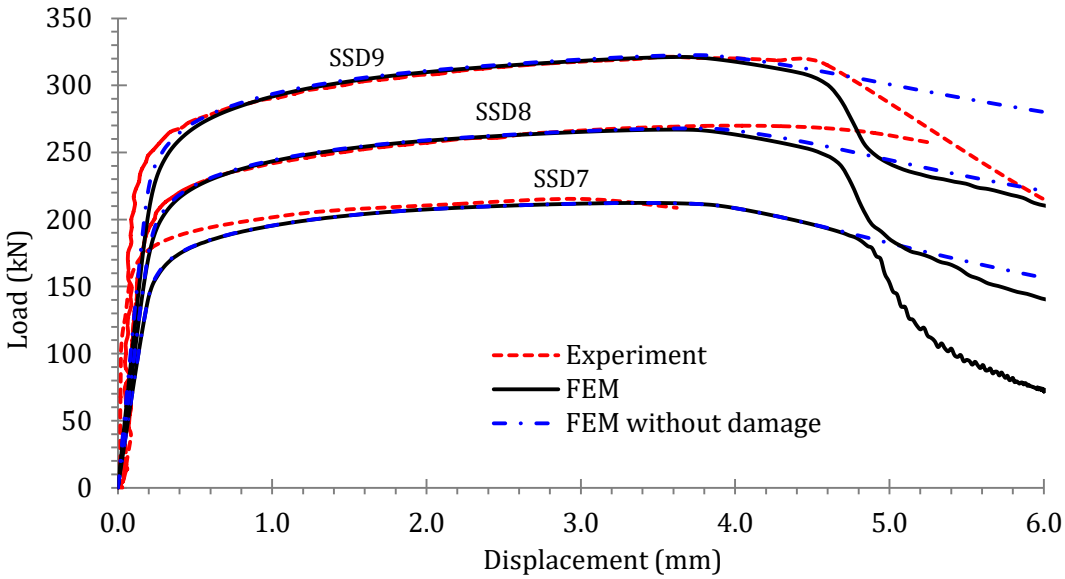

Figure 9 Load versus displacement for SSD7, SSD8 and SSD9

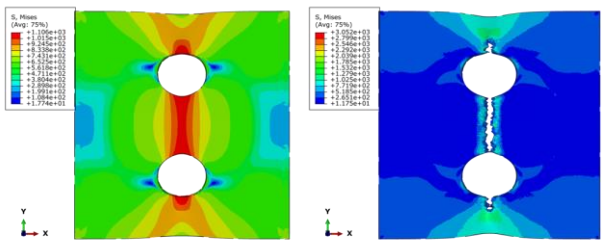

(a)

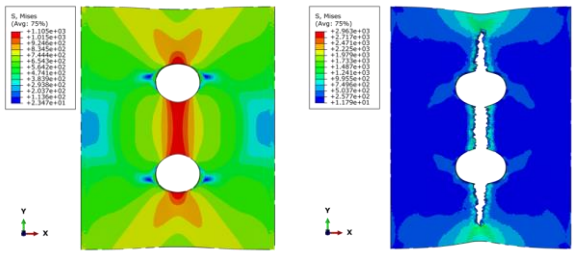

(b)

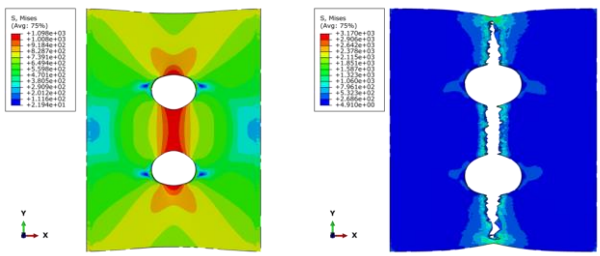

(c)

Figure 10 Von Mises stress and corresponding damage at ultimate load for (a) SSD7, (b) SSD8 and (c) SSD9

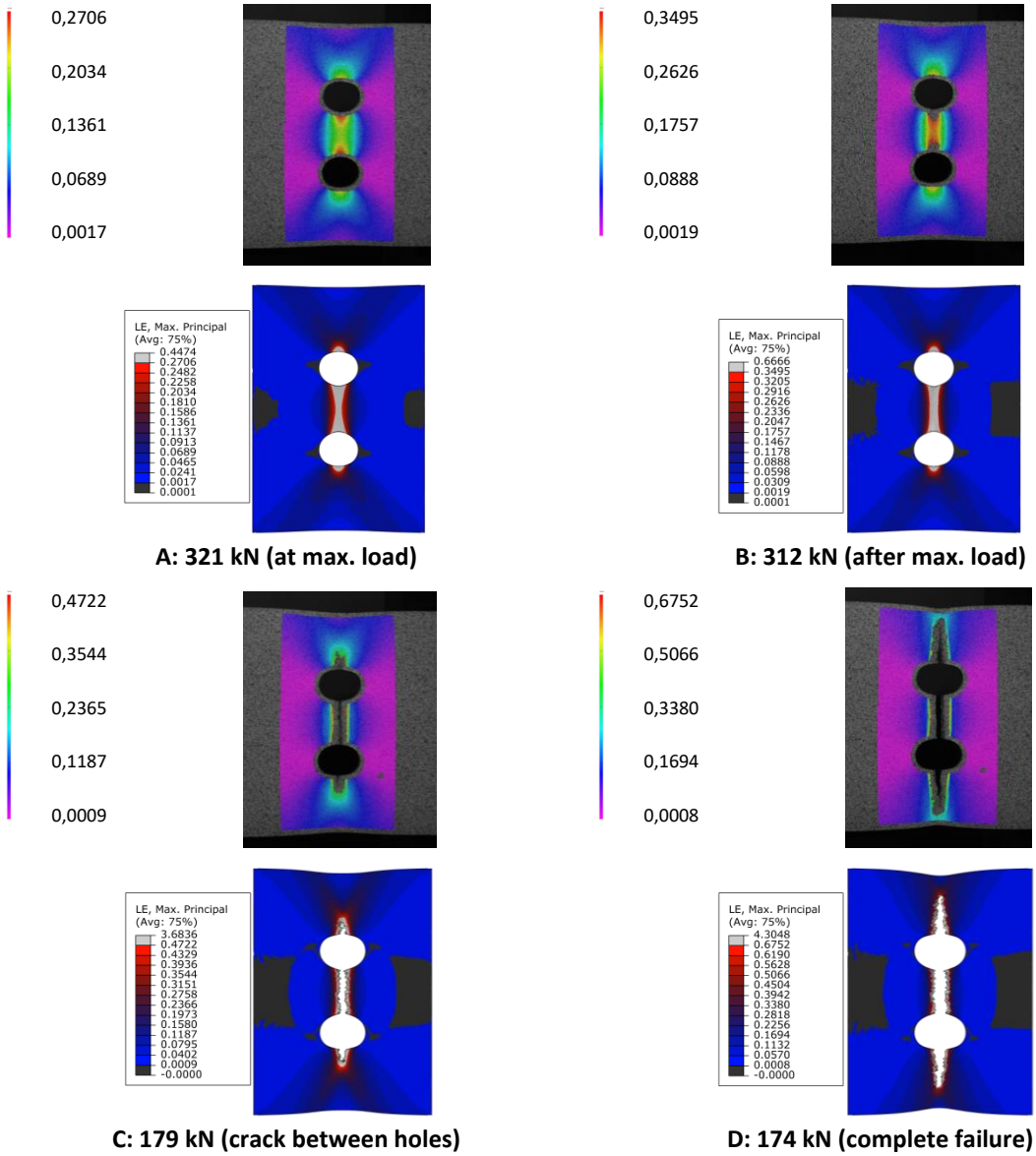

A: 321 kN (at max. load) **B: 312 kN (after max. load)**

C: 179 kN (crack between holes) **D: 174 kN (complete failure)**

Figure 11 Comparisons of the principal logarithmic strains around the bolt holes for SSD9 obtained in experiment and FEM

2.4.2 Bearing failure

The following figures and graphs compare the experiments L-S-1-12 and L-D-1-12 on a single shear and double shear bolted connection tests, respectively (see Figure 12 and Figure 13).

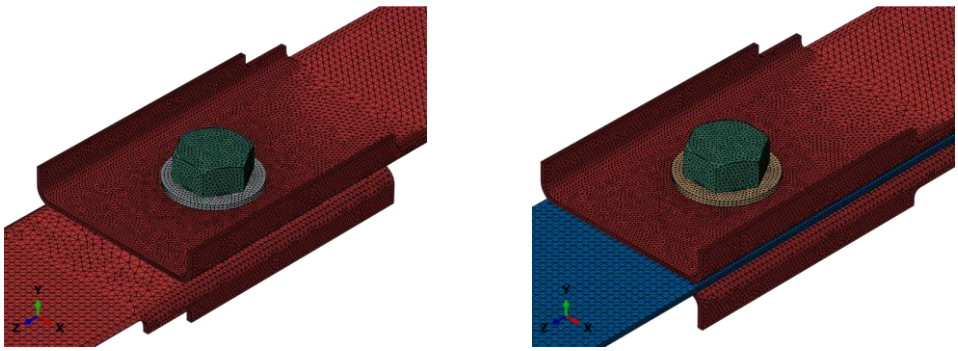

(a) (b)

Figure 12 Components and mesh for (a) L-S-1-12 and (b) L-D-1-12

Note that, in all figures, the experimental average displacement measured by linear variable displacement transducer (LVDT) is compared to the displacement difference of two nodes in the FE model located at the exact same place as the LVDT. The two LVDTs were set-up to measure the elongation of the connection part along a distance of 200 mm [19]. Figure 14 presents comparisons of failure patterns for both lipped plates of the single shear connection as well as the outer and inner plates of the double shear connections. In addition, Figure 14 shows the ductile damage initiation criterion namely DUCTCRT [32] and the scalar damage variable describing the material stiffness degradation namely SDEG [32] after reaching the ultimate connection strength and the damage initiation, for the top plate of L-S-1-12 model and the inner plate of L-D-1-12 model. It can be clearly seen that both models fail by bearing of the connected plates, as evidenced by considerable pilling-up of material in front of the bolt and excessive hole deformation. This causes the state of damage in the elements in the vicinity of the hole to increase (SDEG output > 0) and leads to the removal of the failed elements. The single shear test is relatively well modelled with, however, slightly worse predictions of the failure mode leading to over evaluation of the failure load with an experimental-to-numerical ultimate load ratio of 0.88. The experimental-to-numerical displacement ratio corresponding to the ultimate load $\delta_{u,FEM}/\delta_{u,test}$ is 1.09. The FE model indeed shows different deformations of the bottom plate compared to the experiment. This could be due to the two connection plates that are assumed to be similar while dissimilar in reality, due to the effects of, e.g., the fabrication process, bolt hole drilling and bolt position. The more critical connection plate controlled the ultimate load of the specimen as shown in Figure 14a. The double shear tests are quite accurately modelled both in terms of failure modes, stiffness, ductility and failure loads (load-displacement curve) with an experimental-to-numerical ultimate load ratio of 0.98 this time, and corresponding experimental-to-numerical displacement ratio $\delta_{u,FEM}/\delta_{u,test}$ of 0.85. However, the observed crack line of the inner plate of L-D-1-12 was not captured in the corresponding FE model (see Figure 14b).

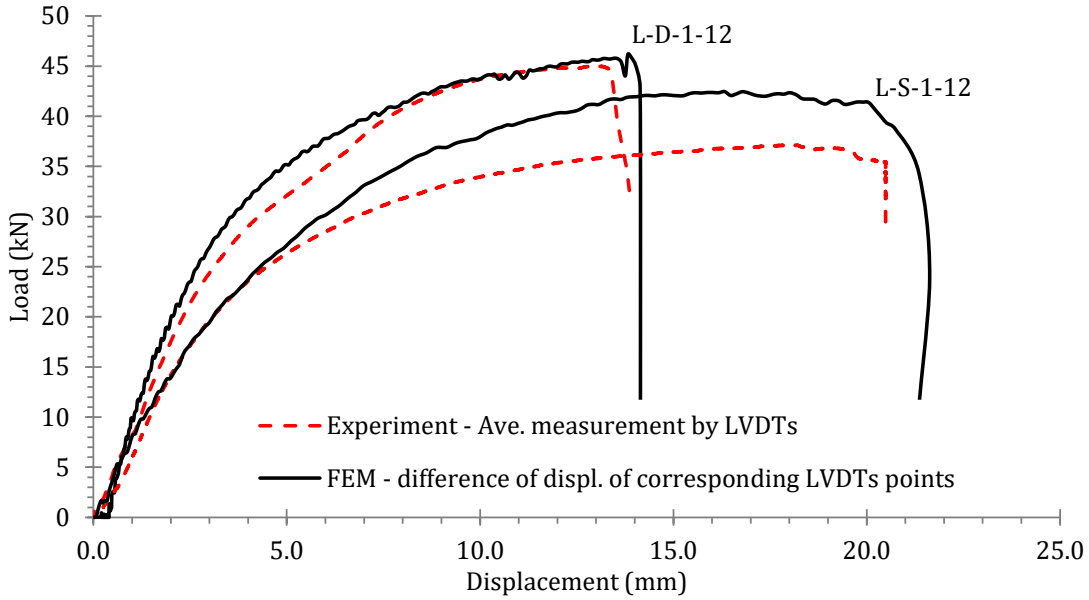

Figure 13 Load versus displacement for L-S-1-12 and L-D-1-12 [19]

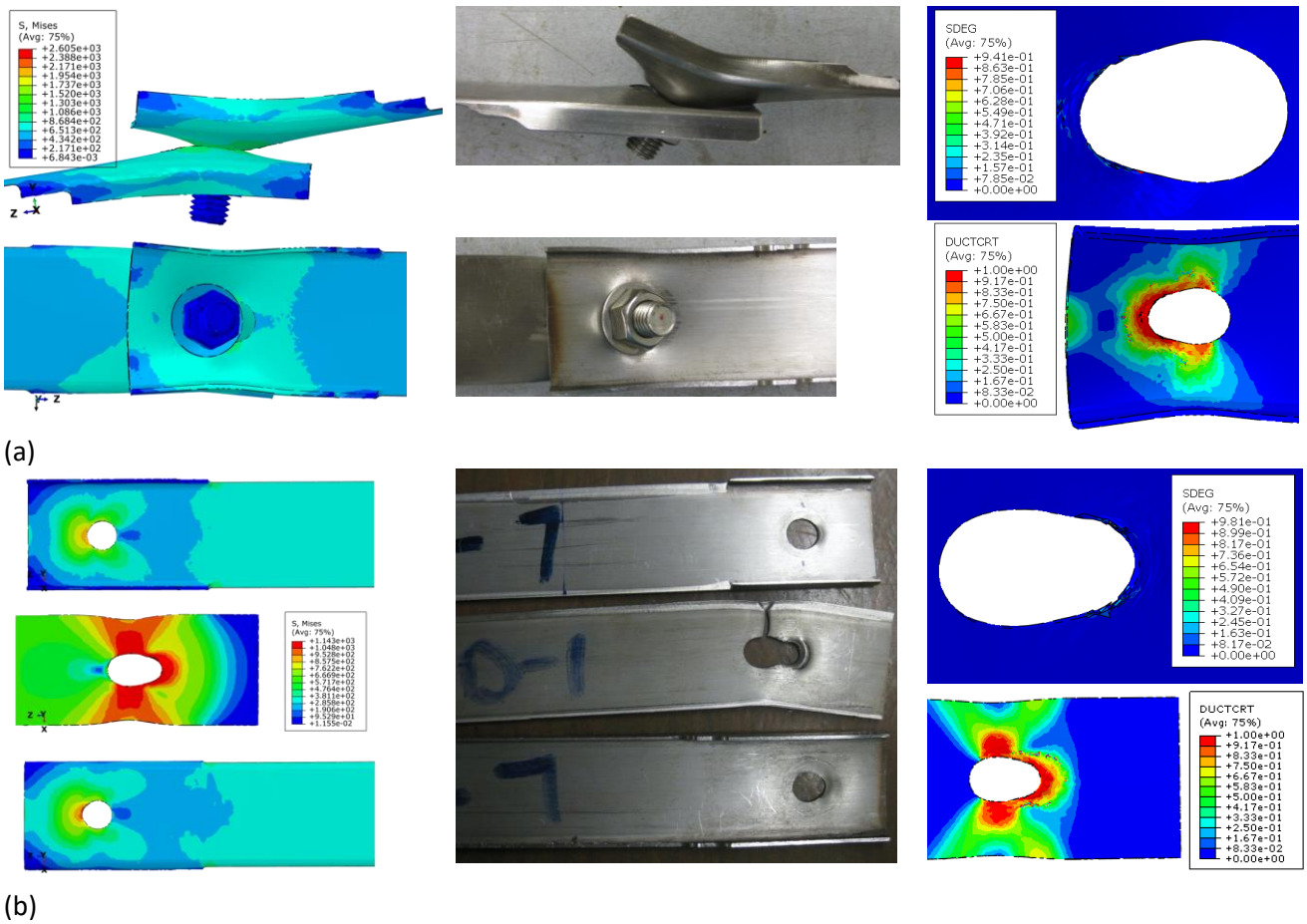

Figure 14 Von Mises stresses at ultimate load and damage outputs after damage initiation for (a) L-S-1-12 and (b) L-D-1-12 and comparison with tests [19]

2.4.3 Combined bearing and net cross-section failure

The following figures and graphs compare the experiments L-D-2Pa-8-r and L-D-2Pe-8 on double shear bolted connection tests, (see Figure 15 and Figure 16).

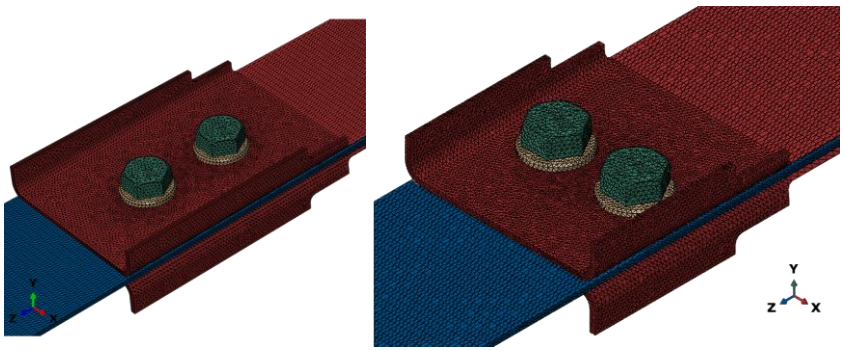

(a) (b)

Figure 15 Components and mesh for (a) L-D-2Pa-8 and (b) L-D-2Pe-8

Both double shear tests show good correlation with the FEM with however a lower initial experimental stiffness. This could be due to the initial bolt position followed by the contacts and then embedment between the bolt threads and bolt hole wall in the test specimens. However, the difference is relatively small, i.e, generally within 0.4 mm under the same load level.

Besides the general connection type and configuration, strength and thickness of the material, several parameters may affect the structural performance of steel connections: a snug-tight condition, the bolt position in the hole, the connection eccentricity and friction coefficient are the most important ones. The frictional forces are developed as a result of the pressure at the interfaces that arises from the bolt tightening. The bolted connection test specimens were tightened by a torque with a constant level of 10 Nm [19]. Since the tightening of the bolts is small, the pre-tension was not considered in the numerical model. The influence of the coefficient of friction between the contact plate surfaces on the behaviour of the tested connections was investigated in this study, on the specimens L-D-2Pa-8-r and L-D-2Pe-8. Three values of the friction coefficient were examined: 0.45, 0.30 and 0.15. Figure 17 depicts this influence, and it indicates that the friction between components affects the connection behaviour mostly in the increasing load regime and after reaching the ultimate connection strength. A higher coefficient of friction leads to a higher initial stiffness. It is seen that the friction has insignificant effects on the ultimate connection strength. However, it can be seen from Figure 17 that the considered coefficients influence the ductility and post-failure behaviour of specimens L-D-2Pa-8-r and L-D-2Pe-8 in different ways. However, this can also be attributed to the numerical solver which includes calibrated fracture parameters for the simulation of ductile damage. Based on these results, a value of μ from 0 up to 0.2 is used and further parametric study will be conducted.

The maximum failure loads are presently very similar with experimental-to-numerical ultimate load ratios of 1.02 and 0.94 for L-D-2Pa-8-r and L-D-2Pe-8 respectively. In addition, the experimental-to-numerical displacement ratios corresponding ultimate loads $\delta_{u,FEM}/\delta_{u,test}$ are 0.92 and 0.97 for L-D-2Pa-8-r and L-D-2Pe-8 respectively.

Figure 18 presents a comparison of the failure patterns for the outer and inner plates of both double shear connections. Very good agreement between the experimental and numerical failure modes was achieved.

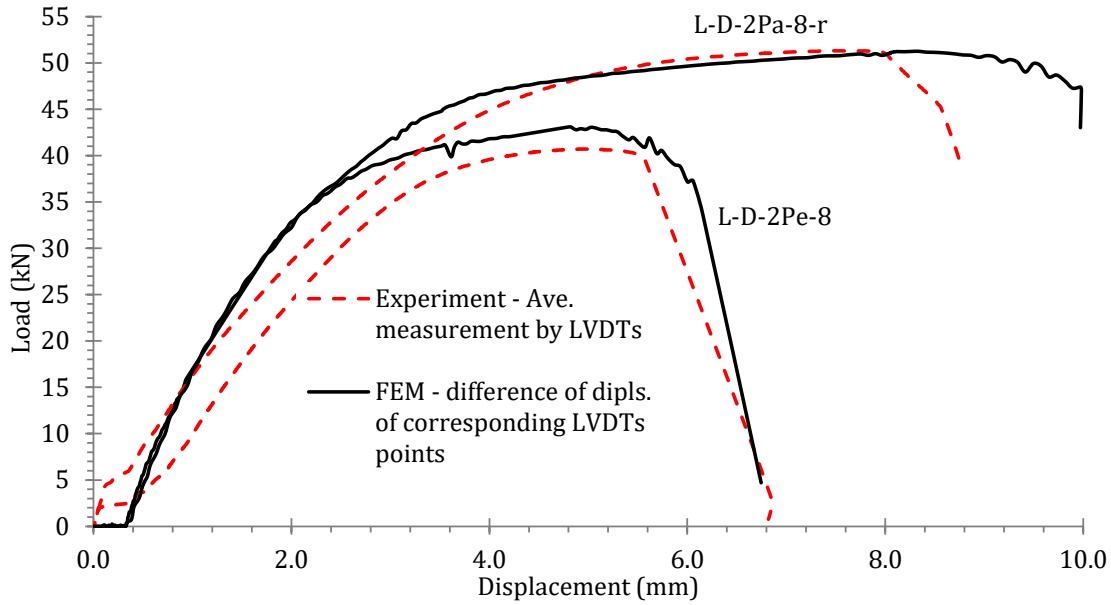

Figure 16 Load versus displacement for L-D-2Pa-8-r and L-D-2Pe-8 [19]

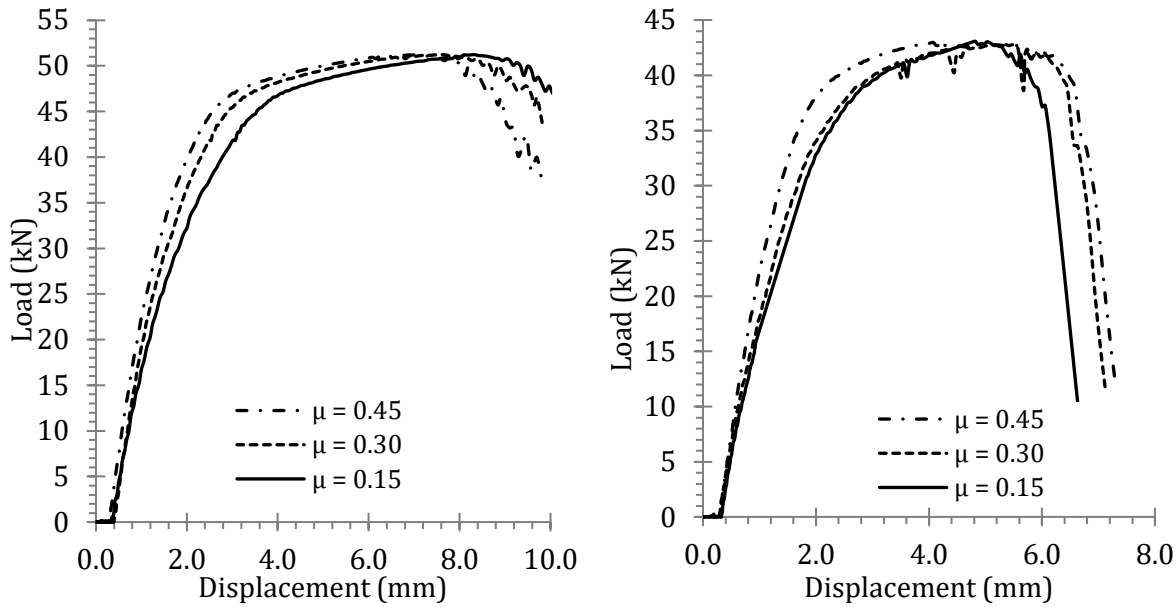

Figure 17 Influence of friction coefficient on load-displacement curves for FE models L-D-2Pa-8-r and L-D-2Pe-8

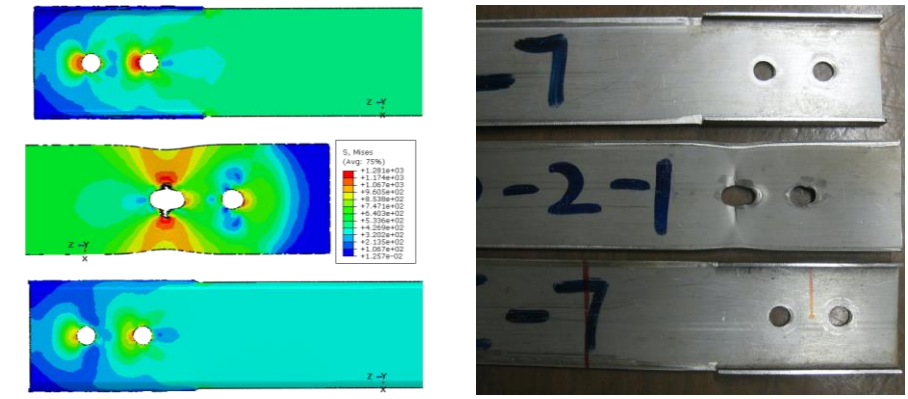

(a)

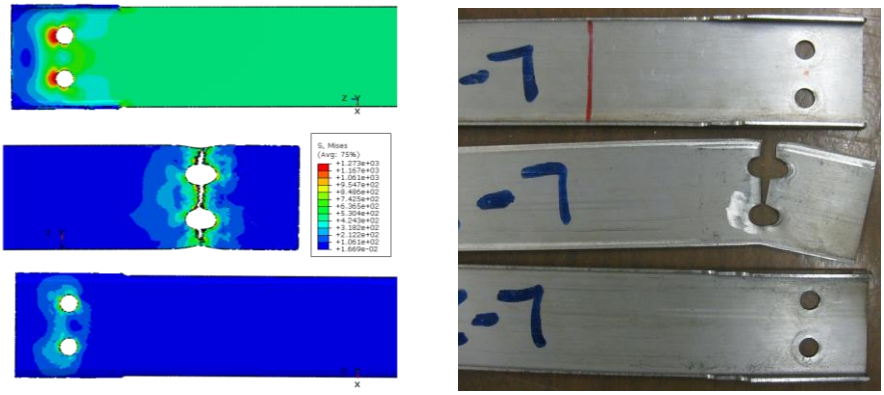

(b)

Figure 18 Von Mises stress and corresponding damage at ultimate load for (a) L-D-2Pa-8-r and (b) L-D-2Pe-8 and comparison with tests [19]

The FE model of the single shear test on a three-bolted connection with staggered bolt spacing, named L-S-3-8, as seen in Figure 19, shows again good correlation with however once again a slightly lower initial experimental stiffness, see Figure 20. The experimental-to-numerical ultimate load ratio is 1.01 and, as can be seen in Figure 21, very similar failure modes. the experimental-to-numerical displacement ratios corresponding ultimate loads $\delta_{u,FEM}/\delta_{u,test}$ is 1.04.

Figure 19 Components and mesh for L-S-3-8

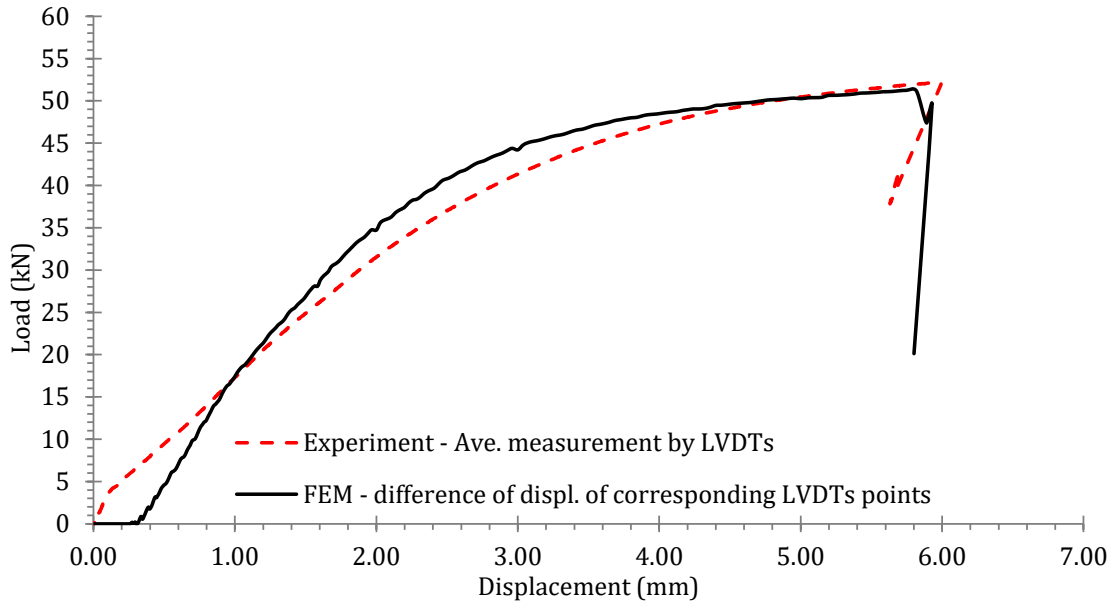

Figure 20 Load versus displacement for L-S-3-8 [19]

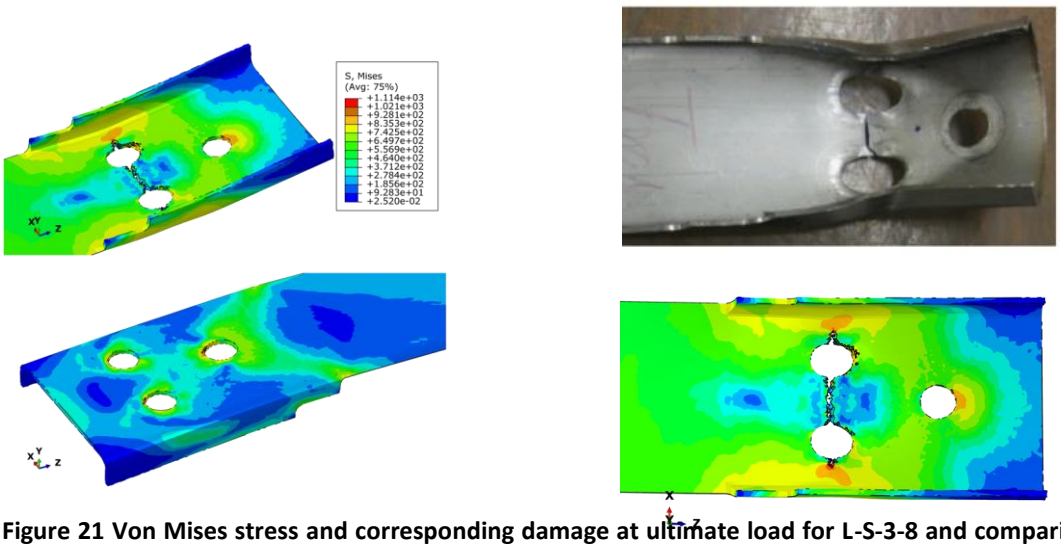

Figure 21 Von Mises stress and corresponding damage at ultimate load for L-S-3-8 and comparison with test [19]

Unlike the previous experiments, the additional bolt prevents initial sliding, as can be seen when both experimental curves are compared (dashed lines, Figure 22). In addition, as previously mentioned, the configuration L-S-3-8 is again characterised by a lower stiffness when compared to the numerical equivalent, as can be seen in Figure 22. In this figure, note that the experimental force-deformation curves are almost parallel after the initial slip.

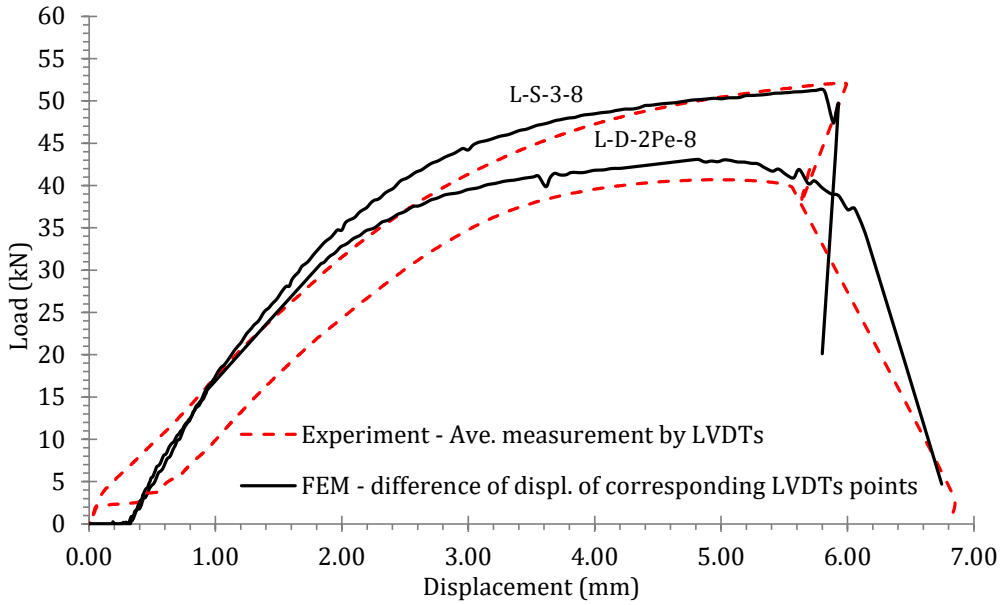

Figure 22 Load versus displacement for L-D-2Pe-8 and L-S-3-8 [19]

3 Parametric study

3.1 Range of studied configurations and geometries

In general, the structural behaviour of bolted connections in cold-formed steel structures is different from that of conventional hot-rolled or fabricated (welded) structures, mainly because of the thinness of the connected parts. It should be noted that the duplex stainless steel of grade EN 1.4162 (i.e., lean duplex) is a relatively new material. Up-to-date, limited investigation on duplex stainless steel grade EN 1.4162 bolted connections has been conducted, in particular for the structural performance of different failure modes. Hence, a detailed parametric study on duplex stainless steel (grade EN 1.4162) bolted connections is conducted in this paper. The study mainly focused on different failure modes in order to assess the corresponding different design equations in current codes.

In order to investigate the structural behaviour of cold-formed duplex bolted connections considering different influencing parameters, the validated FE models are employed to conduct a parametric study. The same grade of stainless steel considered previously is investigated i.e., the lean duplex grade EN 1.4162 and bolt grade A4-80. As discussed in Section 1 of this paper, the strength and failure modes of bolted connections are affected by many factors, such as diameter and number of bolts, bolt arrangement, steel plate thickness, bolt hole spacings, distance between bolt hole centre to plate edges, etc. Hence, the investigated parameters include the end distance e_1 ($1.0d_0$, $1.2d_0$, $1.5d_0$, $2.0d_0$, $2.5d_0$, $3.0d_0$ and $4t$+40), the edge distance e_2, the spacing p_1 ($2.2d_0$, $3d_0$, $5d_0$), the bolt dimeter d (8 mm and 12 mm), the bolt number n (1, 2, 3 and 4) and the thickness of the plate t (1.45, 1.46, 1.47 and 3.0 mm). It is worth noting that the values of end distance ratios e_1/d_0 and spacing ratios p_1/d_0 and p_2/d_0 are out of the range of validity of EN 1993-1-3 [11] (where bolted connections between thin plates with thicknesses $\leq$ 3.0 mm are provided) and AS/NZS 4673 [7]. The geometry and layout of each connection are carefully selected to maintain the predictions of fracture established previously, and

to avoid shearing of the bolts. In total, 133 numerical models are developed and analysed in this section.

The models in the parametric study do not include either the initial geometric imperfections or the load eccentricity. Each model is considered to be a concentrically loaded connection. Bolts are located centrally into the holes with a uniform clearance of 1.0 mm and 2.0 mm for bolt diameter of 8 mm and 12 mm, respectively. To examine the effect of the key parameters on the capacity of shear bolted connections, the configurations shown in Figure 23a (single bolt shear connections) and Figure 23b (double bolt shear connections) are adopted in this parametric study. The designations of FE models in numerical parametric study are as in experiment [19]: the first letter indicates the stainless steel alloy, herein "*L*" for lean duplex; the second letter represents the connection type, where "*S*" represents single shear bolted connection and "*D*" represents double shear bolted connection; the third segment of the label defines the number of bolt and bolt arrangement. If the specimen is assembled by two bolts, then the letters "*Pa*" mean that bolts are arranged parallel to the loading direction, while "*Pe*" mean that bolts are arranged perpendicular to the loading direction. The fourth part of the label, "*d*", is the nominal diameter of the bolt used in the connection and the last symbol, "t_e", is the thickness of the external connection plate. In addition, "*b*" is the width of connection plate; "$L_{1,e}$" is the length of the external connection plate; "$L_{1,i}$" is the length of the internal (middle) plate for double shear connections; "t_i" is the thickness of the internal connection plate and "d_0" is the hole diameter.

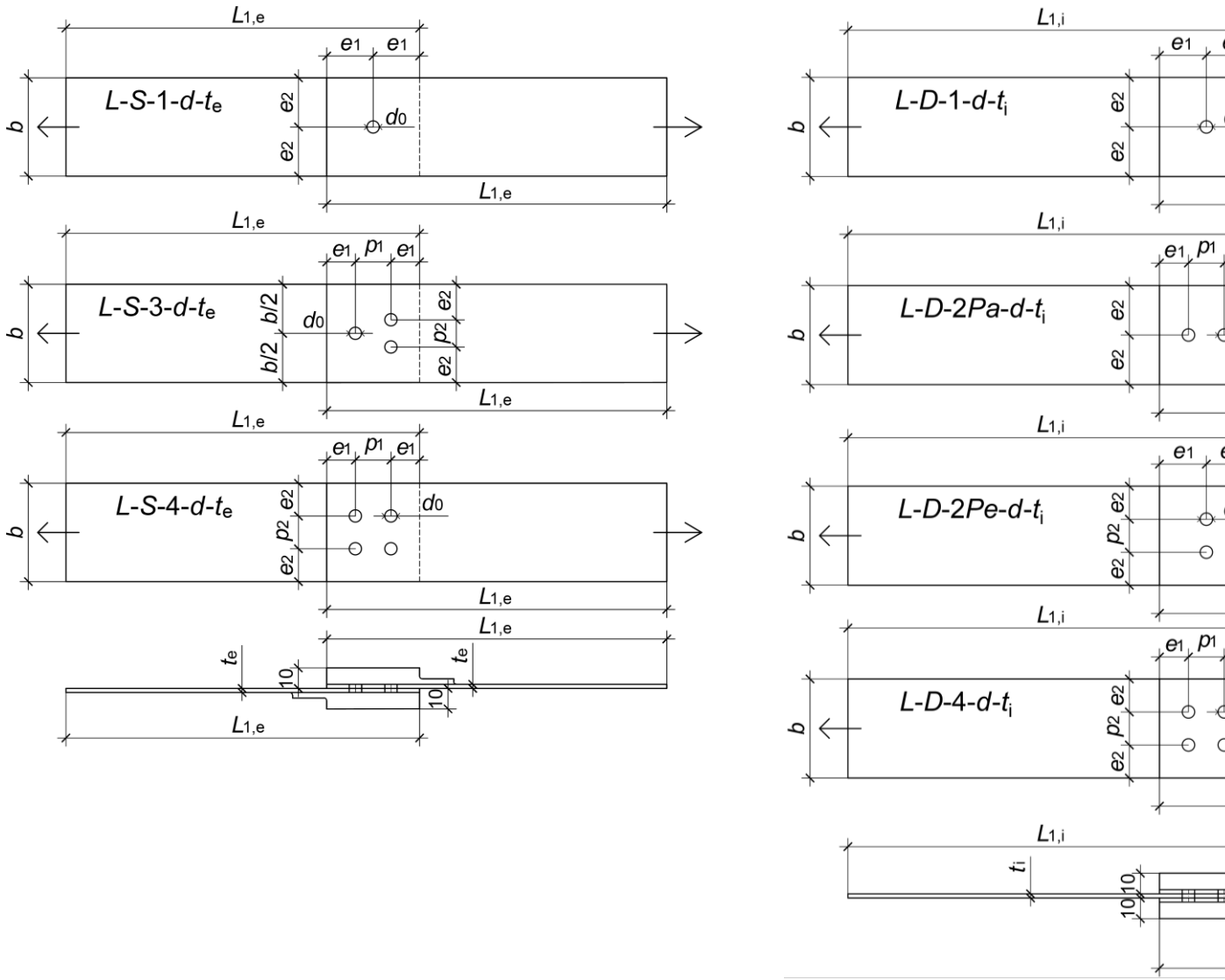

(a) single bolt shear connections (b) double bolt shea

Figure 23 Nominal geometry and parameter designation of FE models in parametric study (all dimensions are in mm)

3.2 Results and comparison with design standards

This section provides the results of the numerical parametric study and the comparison between the numerically obtained ultimate capacities and the corresponding predicted values in accordance with the Eurocodes EN 1993-1-3 [11], EN 1993-1-8 [10] and the Australian/New Zealand Specifications AS/NZS 4673 [7]. The design equations in AISC [6] were not used for the strength predictions as they are provided for carbon steel bolted connections. The equations provided by EN 1993-1-8 [10] were used in this study, as it is stated in Eurocode 3 Part 1.4 [5] that the provisions given in EN 1993-1-8 [10] are applicable to stainless steels, except where modified or superseded in [5].

It should be emphasized here that the ultimate strengths of the shear bolted connections in numerical parametric study do not include impact of possible initial geometric imperfections and load eccentricity. Note that the design equations for bolted connections provided in the SEI/ASCE Specification [8] are identical to those in the AS/NZS Standard [7]. Clause 6 of Eurocode 3 Part 1.4 [5] provides the design provisions for stainless steel connections, with no distinction being made between thin and thick plated connections. Considering the range of validity of the design recommendations stated in Table 8.4 of EN 1993-1-3, the FE results gained on connections with plate thicknesses less than 3 mm are compared with the EN 1993-1-3 design predictions. Whereas for connections with plate thickness equal to 3 mm, the comparisons are made with EN 1993-1-8. Regarding the design criteria stated in AS/NZS 4673, there is no explicit recommendation separating thin and thick plates.

The numerical results obtained during this parametric study were carefully analysed to clearly identify the failure mode of each FE model, observing its deformation and fracture mode. Depending on the chosen connection configuration and geometry, the following types of failure occurred: (i) longitudinal shear (tear out) failure of the plate in the line of applied load, (ii) bearing of the plate (in front of the bolt), (iii) net section failure (tearing of the plate in the net section) and (iv) block tearing failure. Considering the distribution of material damage namely DUCTCRT [32] in the post-failure regime, these failure modes are respectively illustrated in Figure 24, Figure 25, Figure 26 and Figure 27 for four selected FE models.

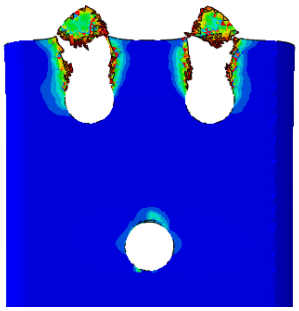

L-S-3-8-1.46
e_1/d_0 = 1.2; p_1/d_0 = 3.0; p_2/d_0 = 2.4

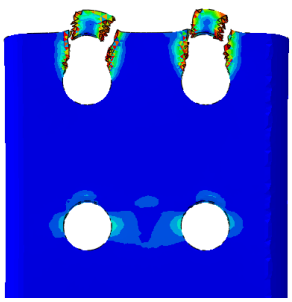

L-S-4-8-1.46
e_1/d_0 = 1.0; p_1/d_0 = 3.0; p_2/d_0 = 2.4

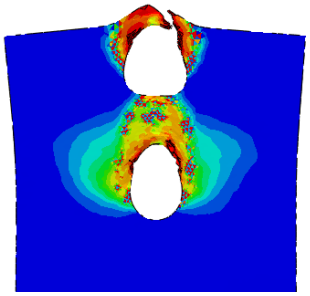

L-D-2Pa-8-1.45
e_1/d_0 = 1.0; p_1/d_0 = 2.2

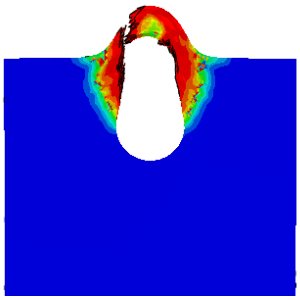

L-D-1-12-3
e_1/d_0 = 1.0

Figure 24 Longitudinal shear (tear out or combined tear out and bearing) failure

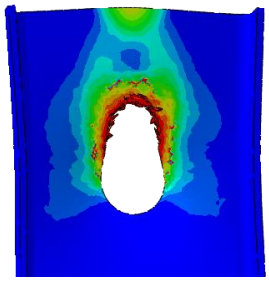

L-S-1-12-1.5
e_1/d_0 = 2.5

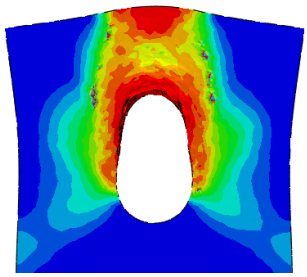

L-D-1-12-1.5
e_1/d_0 = 2.0

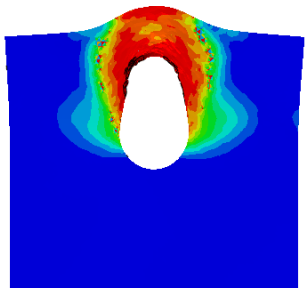

L-D-1-12-3
e_1/d_0 = 1.5

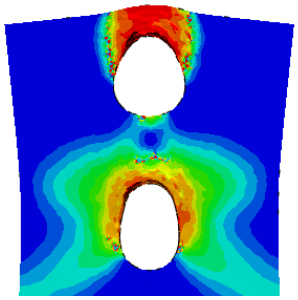

L-D-2Pa-12-3
e_1/d_0 = 1.2; p_1/d_0 = 2.2

Figure 25 Bearing failure

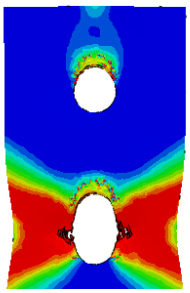

L-D-2Pa-12-3
e_1/d_0 = 2.0; p_1/d_0 = 3.0

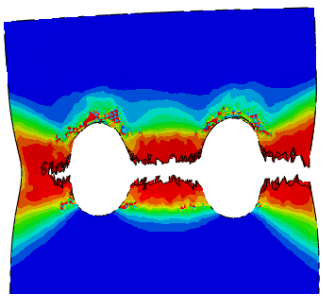

L-D-2Pe-8-1.45
e_1/d_0 = 2.5

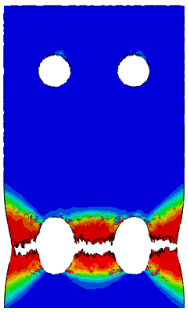

L-D-4-8-1.45
e_1/d_0 = 2.0; p_1/d_0 = 5.0; p_2/d_0 = 2.4

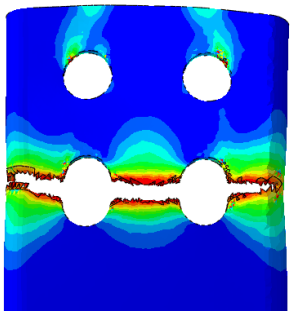

L-S-4-8-1.46
e_1/d_0 = 1.5; p_1/d_0 = 2.2; p_2/d_0 = 2.4

Figure 26 Net section failure

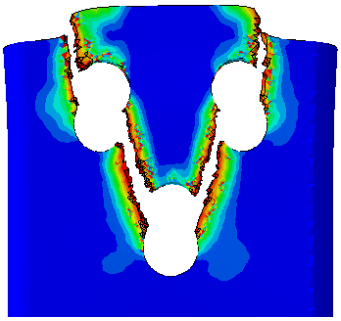

L-S-3-8-1.46
e_1/d_0 = 1.5; p_1/d_0 = 2.2; p_2/d_0 = 2.4

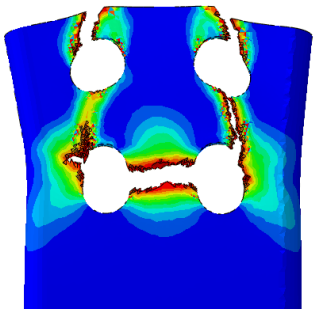

L-S-4-8-1.46
e_1/d_0 = 1.2; p_1/d_0 = 2.2; p_2/d_0 = 2.4

Figure 27 Block tearing failure

The FE ultimate strengths are compared with the unfactored connection strengths predicted by the Eurocode 3 [10], [11], Australian & New Zealand structural stainless steel design standard [7] and North American structural stainless steel design standard [8]. To provide relevant comparisons, the same values of material properties (yield strength and ultimate tensile strength, see Table 4) for lean duplex stainless steel EN 1.4162 that were used in numerical test simulations and parametric studies, were taken in determining the design predictive strengths. The EN partial safety factor γ_{M2} and LFRD resistance factor ϕ were taken as 1.0. The design ultimate strength is the minimum strength considering all possible failure modes. The predicted failure mode is the corresponding one.

The accuracy of the EN 1993-1-8, EN 1993-1-3, AS/NZS, SEI/ASCE design equations in comparison to the results from the nonlinear numerical parametric study is illustrated in Figure 28 and Figure 29 for double shear and single shear bolted connections, respectively. Moreover, Figure 30 and Figure 31 present the results of numerical data with respect to the codified predicted data, for double shear and single shear bolted connections, respectively. In addition, the FE ultimate strengths $P_{u,FE}$ and failure modes of all studied connections are provided in more detail in Appendix A, Table A1 and Table A2, respectively.

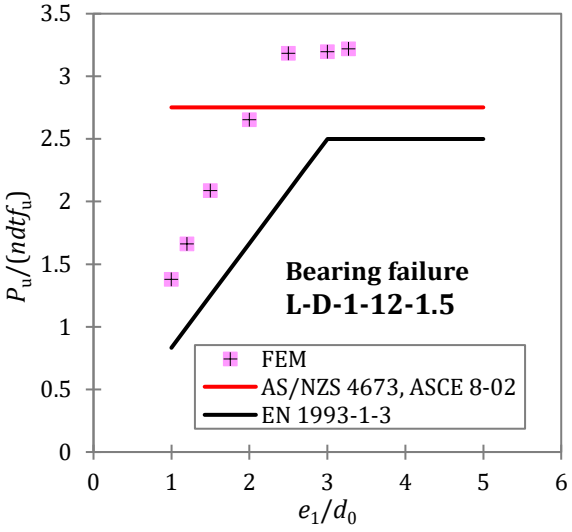

Accuracy assessment of equs. (11) and (14)

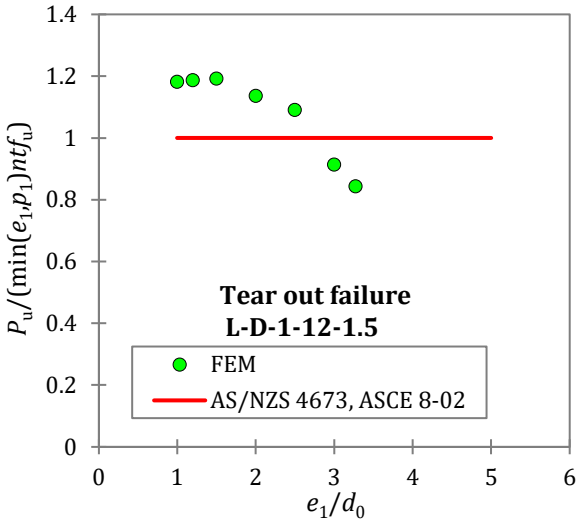

Accuracy assessment of equ. (15)

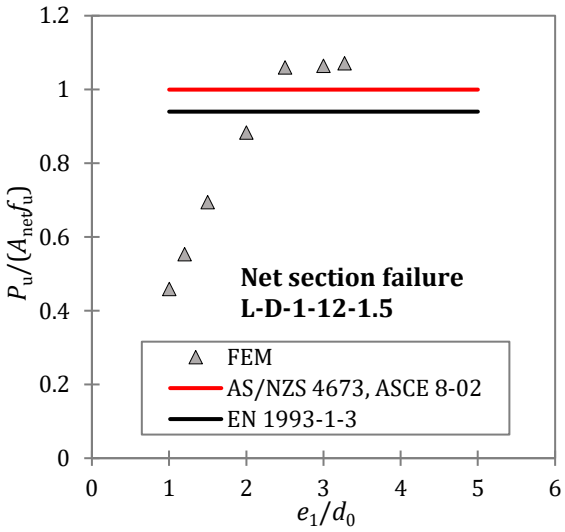

Accuracy assessment of equs. (3) and (6)

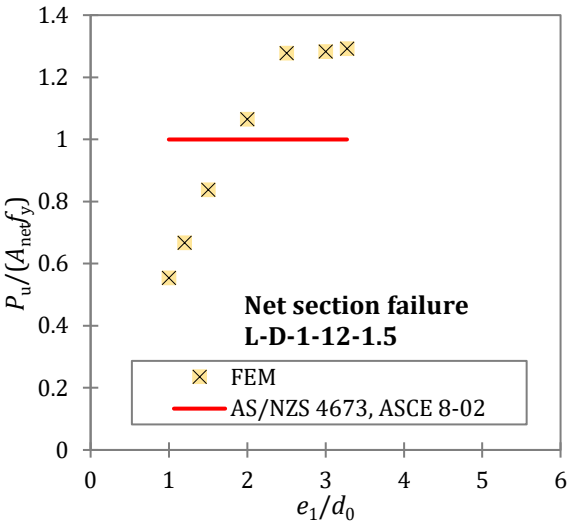

Accuracy assessment of equ. (7)

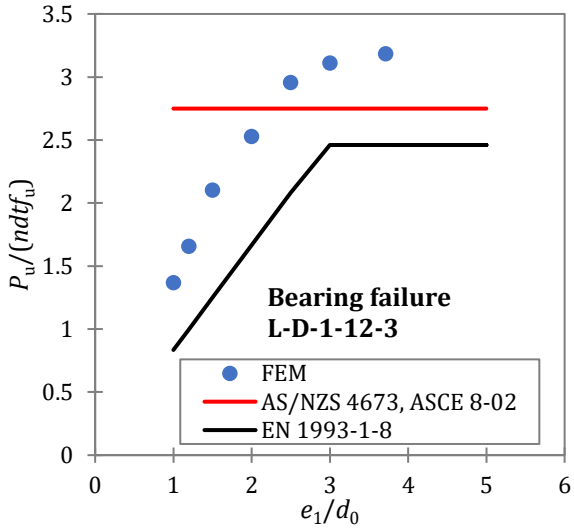

Accuracy assessment of equs. (11) and (14)

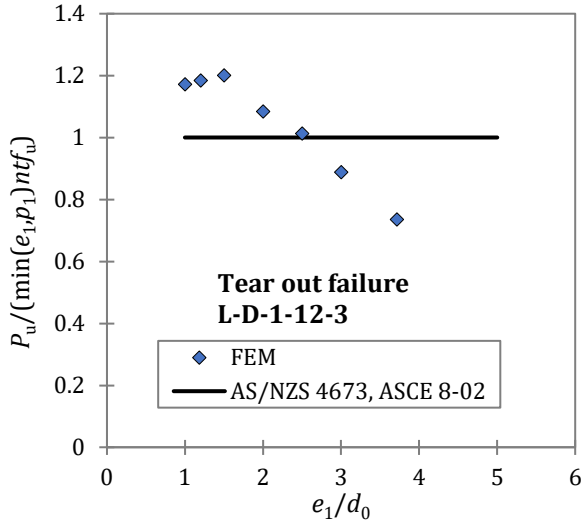

Accuracy assessment of equ. (15)

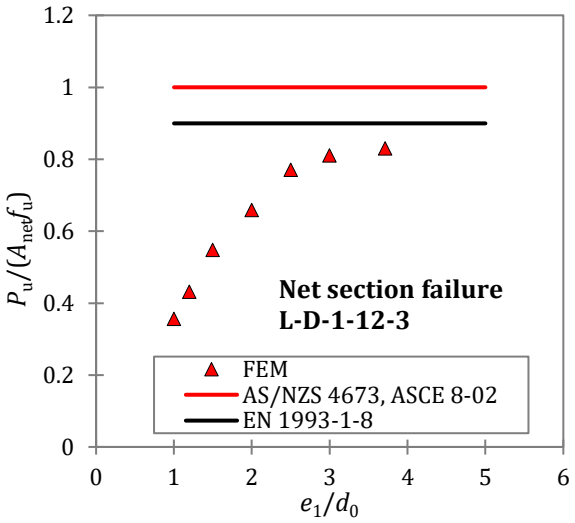

Accuracy assessment of equs. (3) and (6)

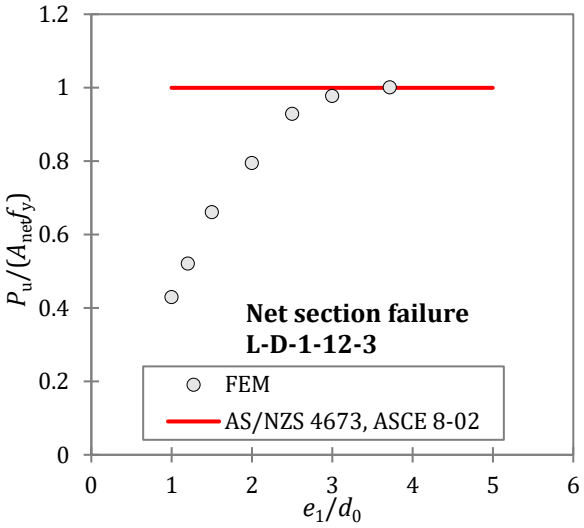

Accuracy assessment of equ. (7)

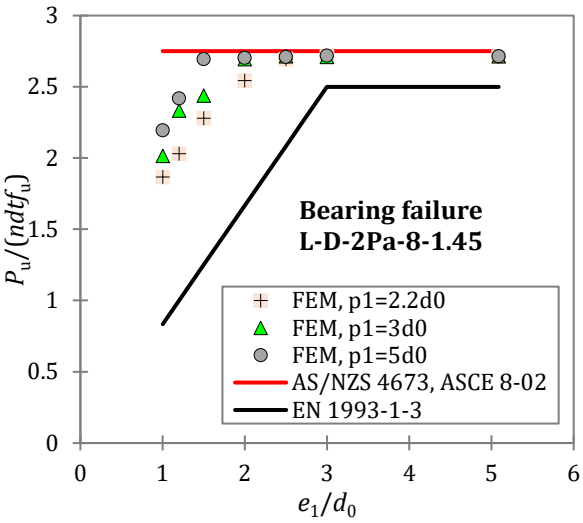

Accuracy assessment of equs. (11) and (14)

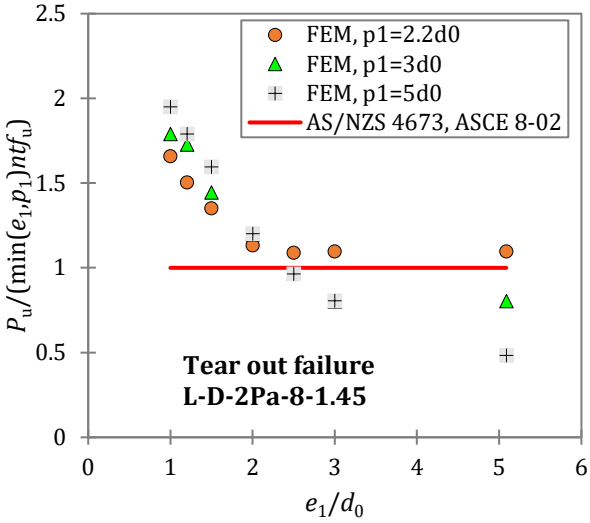

Accuracy assessment of equ. (15)

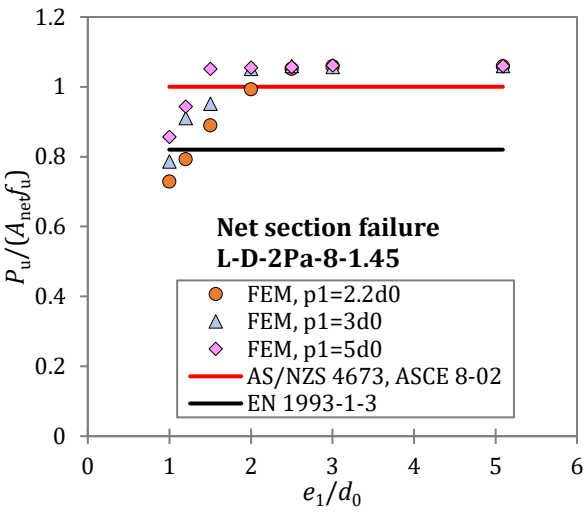

Accuracy assessment of equs. (3) and (6)

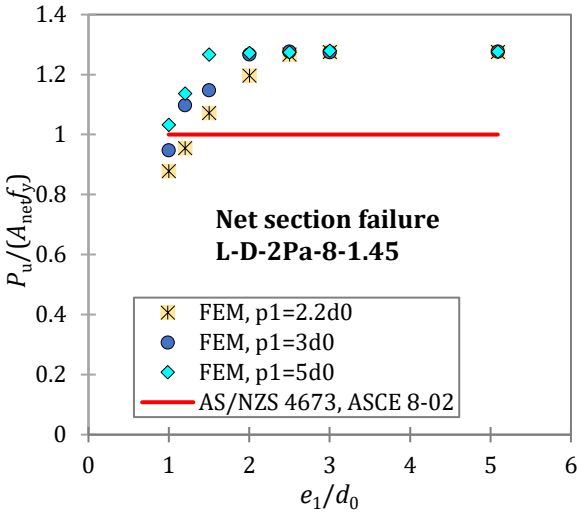

Accuracy assessment of equ. (7)

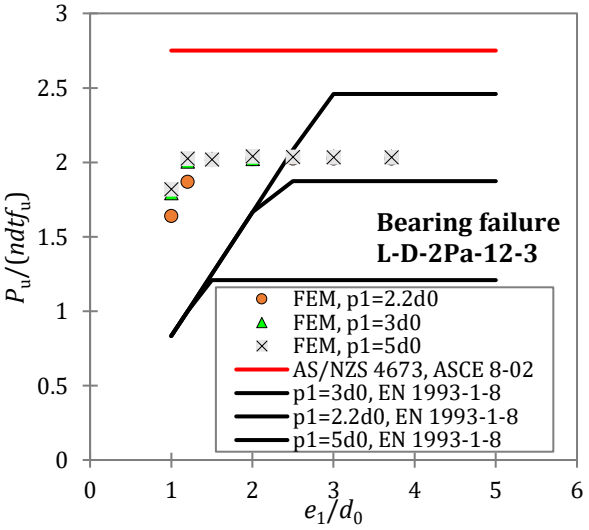

Accuracy assessment of equs. (9) and (14)

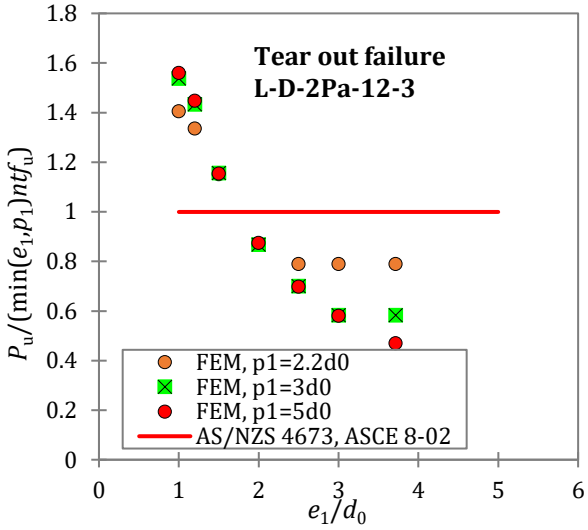

Accuracy assessment of equ. (15)

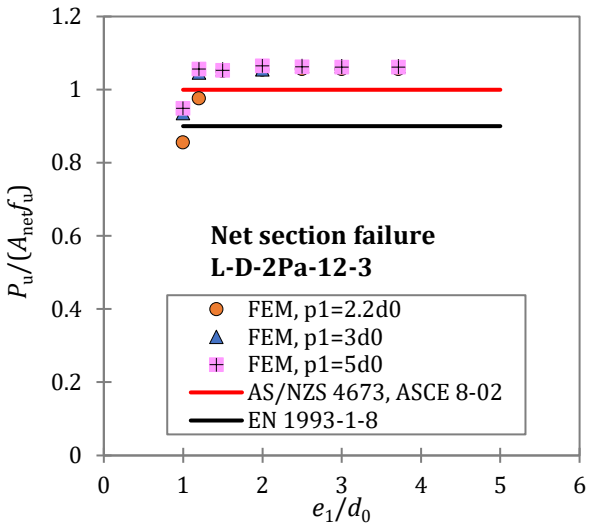

Accuracy assessment of equs. (2) and (6)

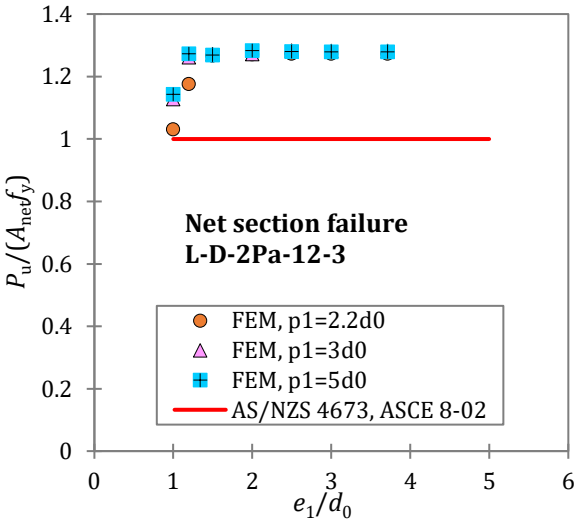

Accuracy assessment of equ. (7)

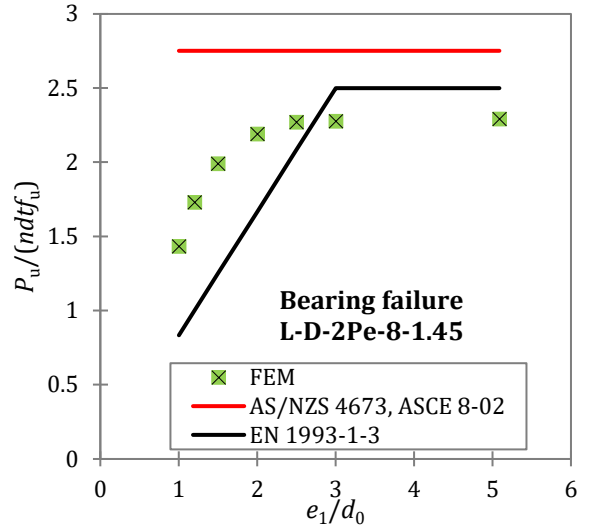

Accuracy assessment of equs. (11) and (14)

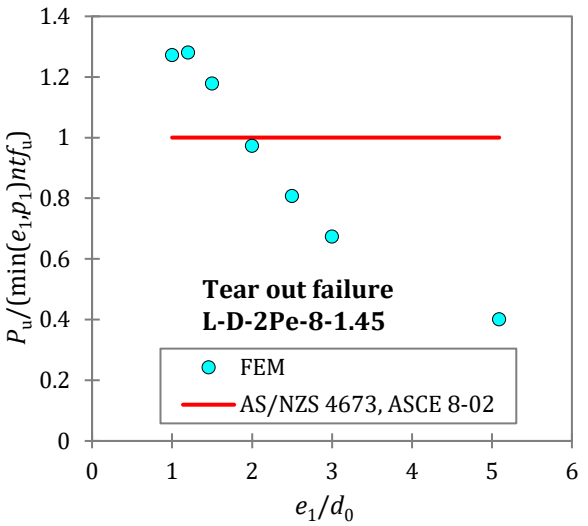

Accuracy assessment of equ. (15)

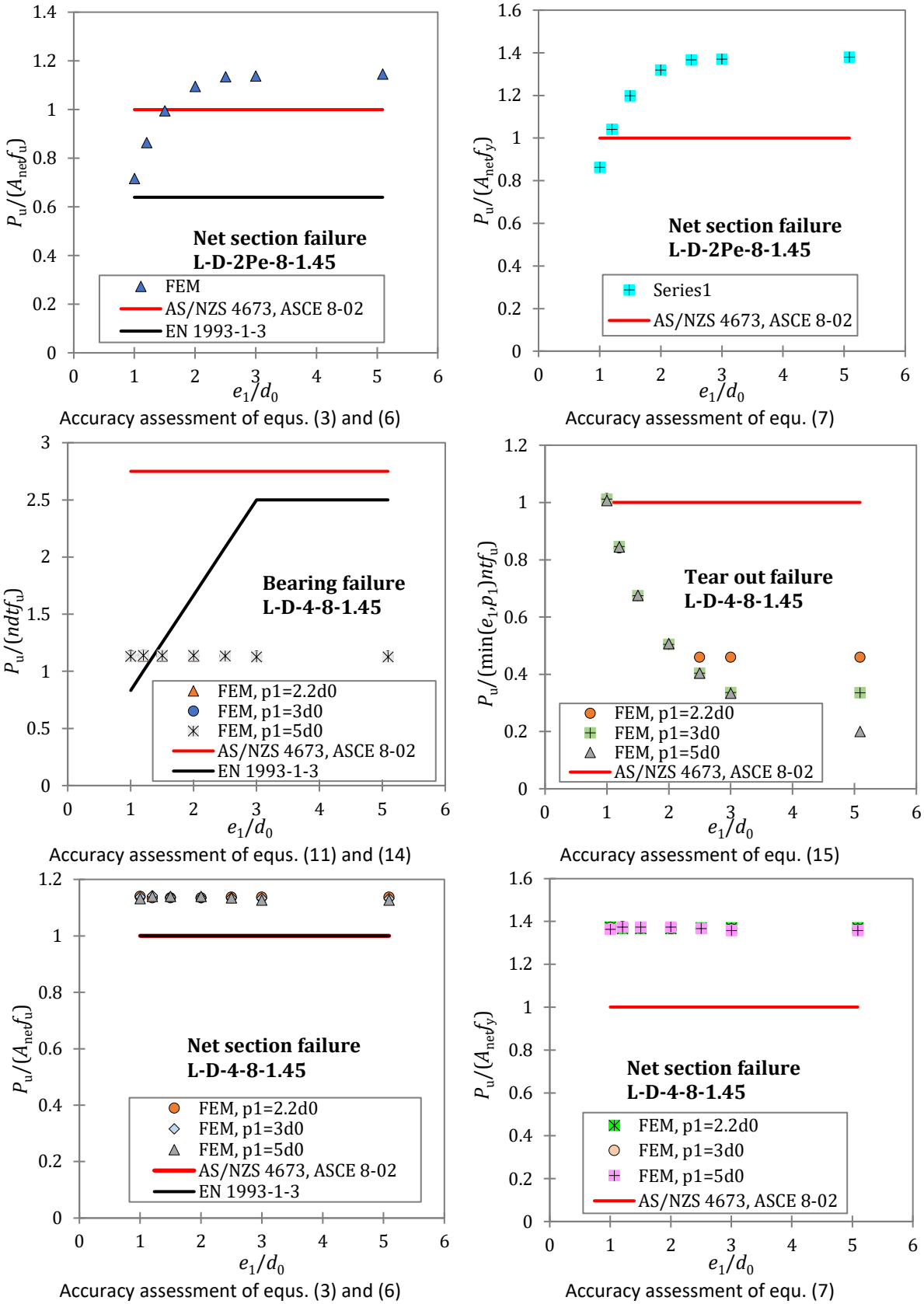

Figure 28 Comparison of numerical data with design predictions for double shear bolted connections.

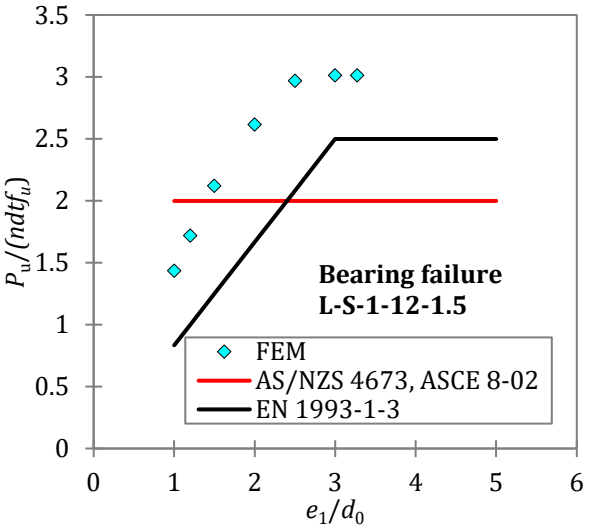

Accuracy assessment of equs. (11) and (13)

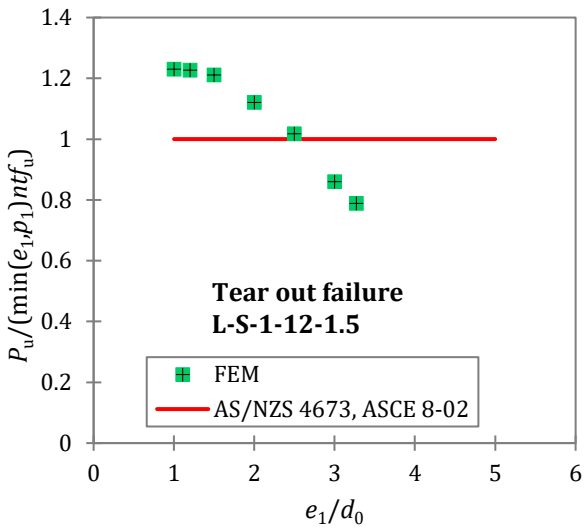

Accuracy assessment of equ. (15)

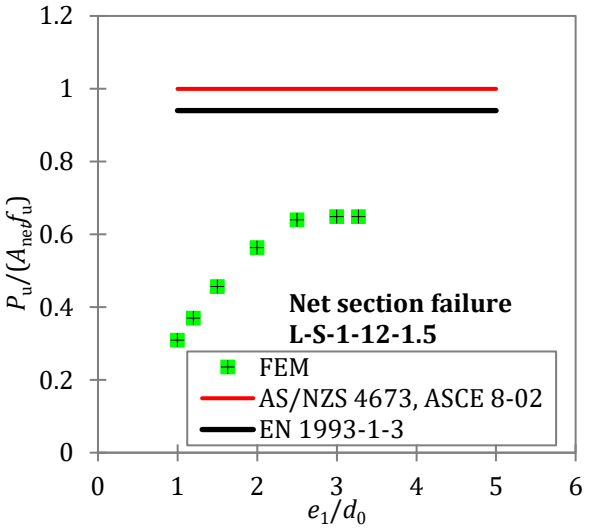

Accuracy assessment of equs. (3) and (6)

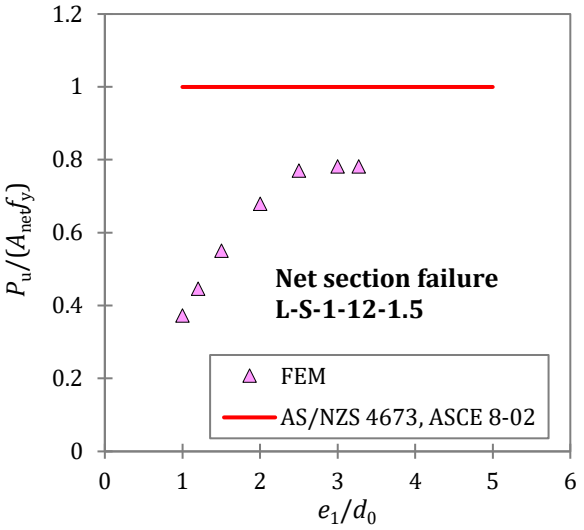

Accuracy assessment of equ. (7)

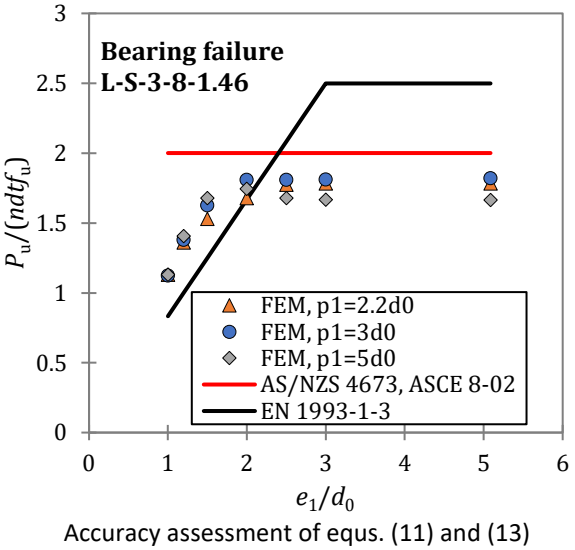

Accuracy assessment of equs. (11) and (13)

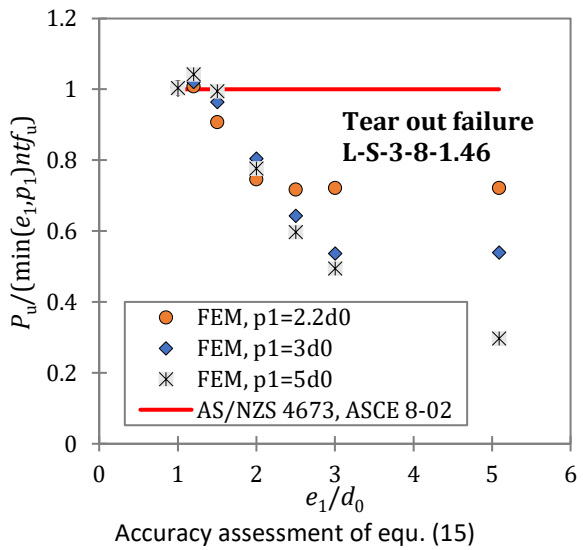

Accuracy assessment of equ. (15)

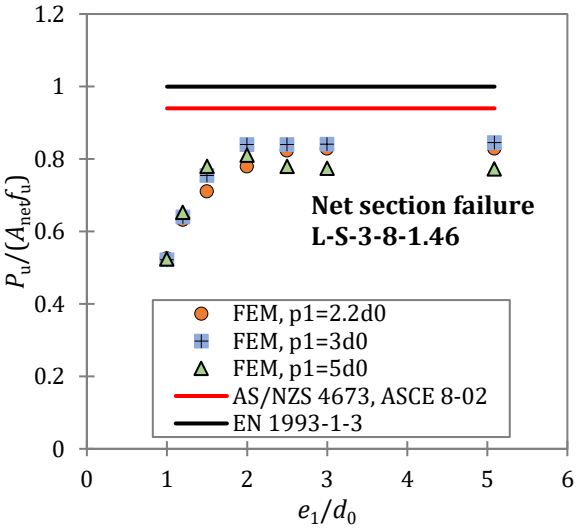

Accuracy assessment of equs. (3) and (6)

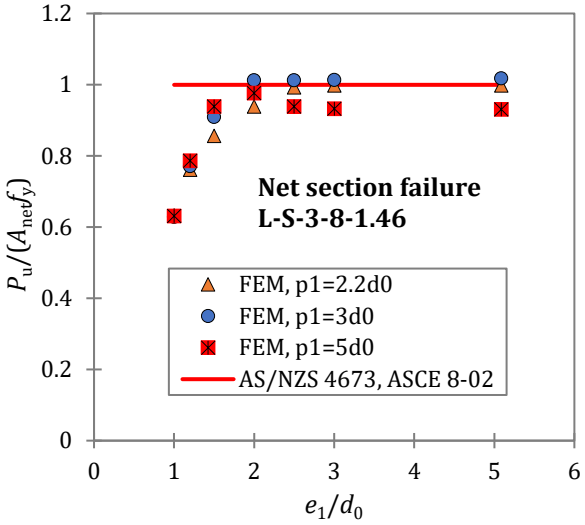

Accuracy assessment of equ. (7)

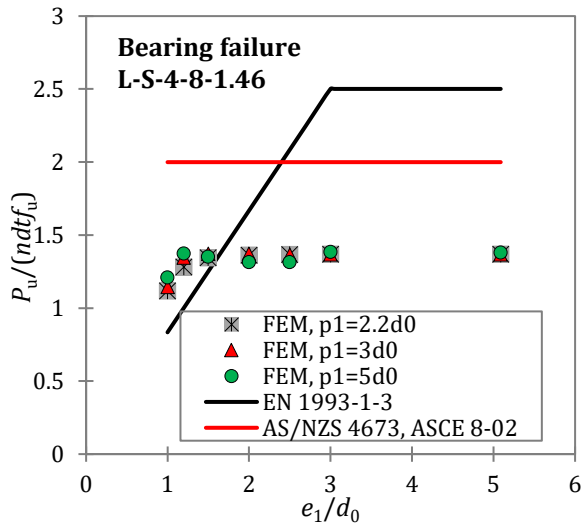

Accuracy assessment of equs. (11) and (13)

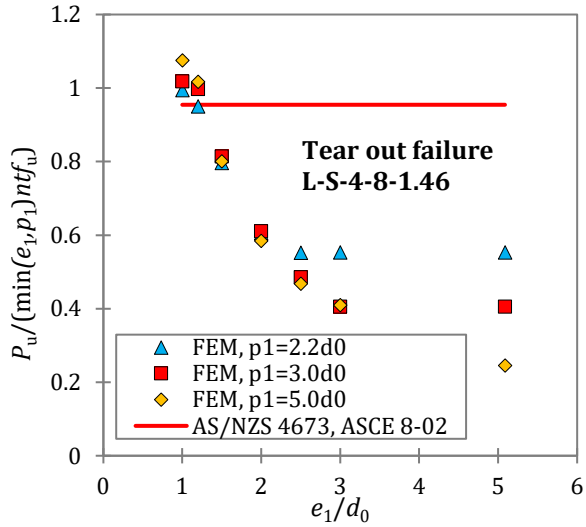

Accuracy assessment of equ. (15)

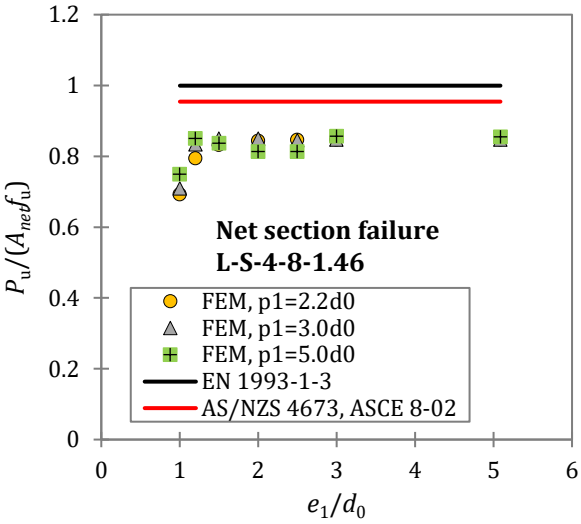

Accuracy assessment of equs. (3) and (6)

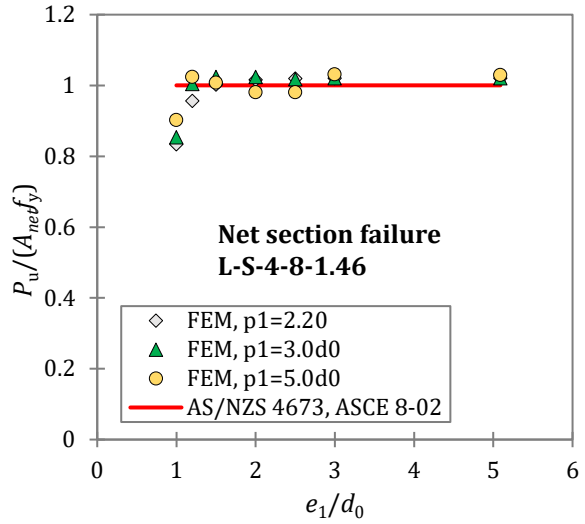

Accuracy assessment of equ. (7)

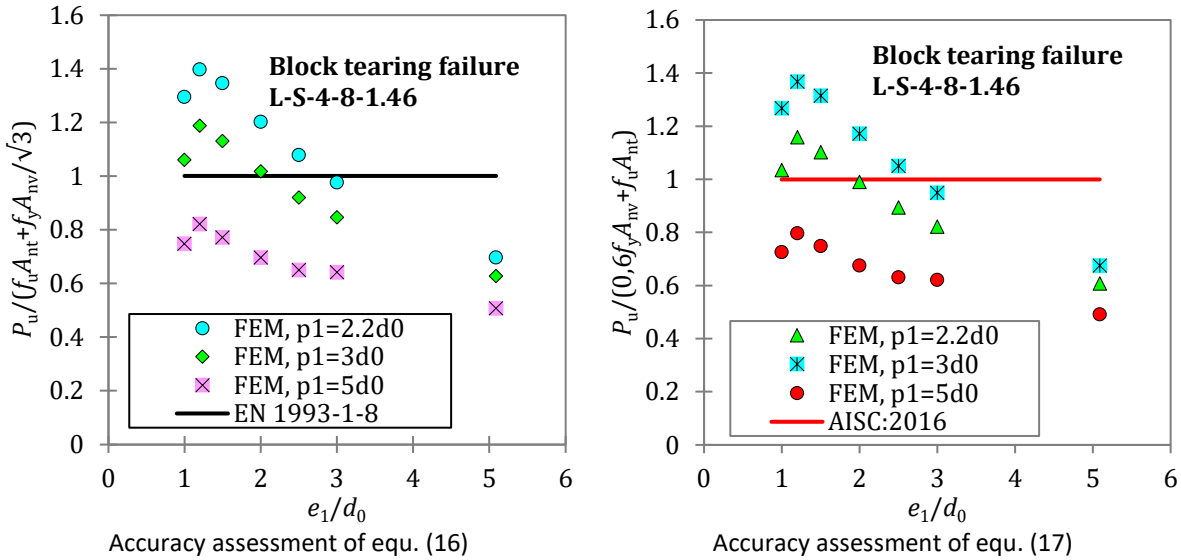

Figure 29 Comparison of numerical data with design predictions for single shear bolted connections

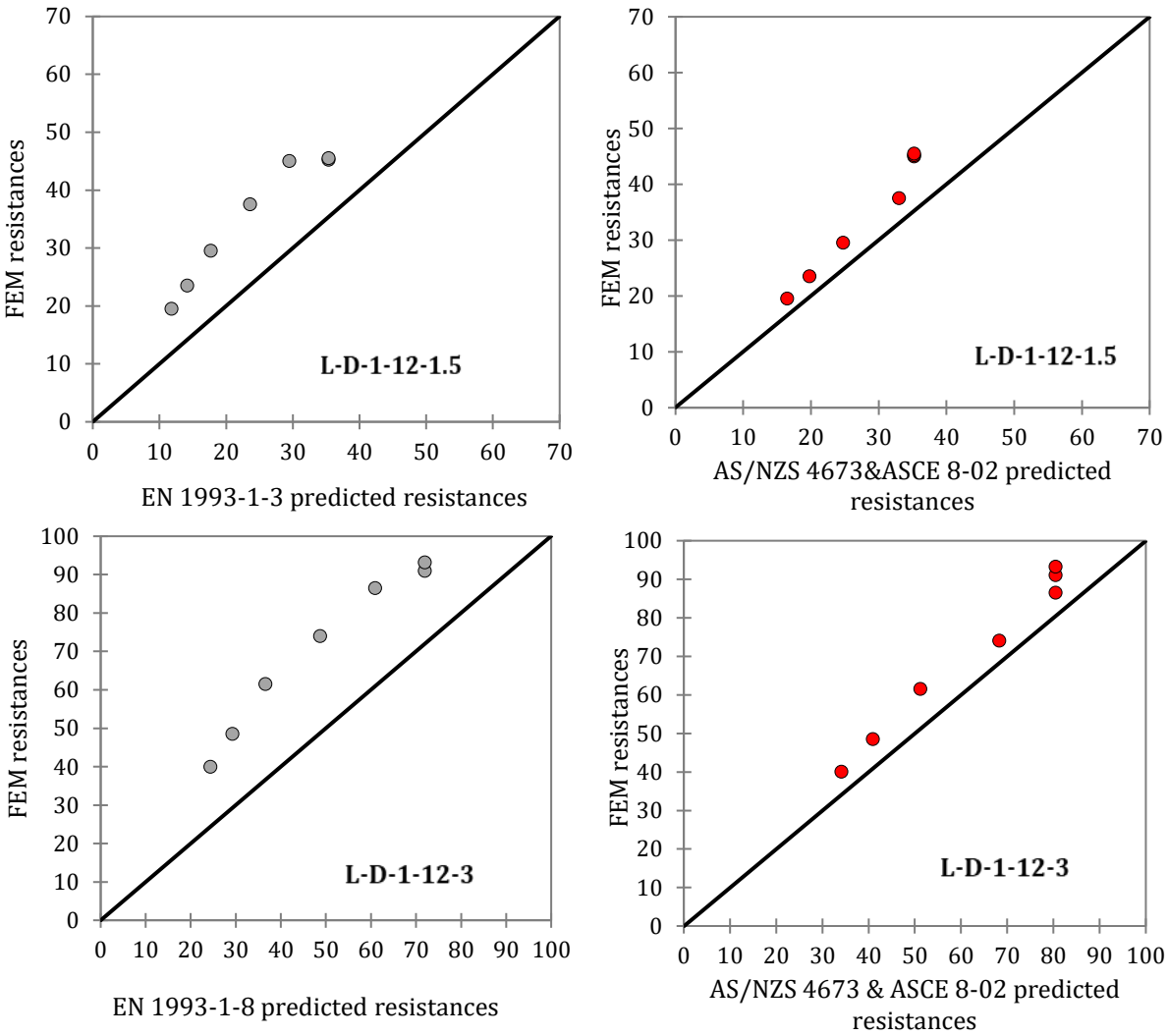

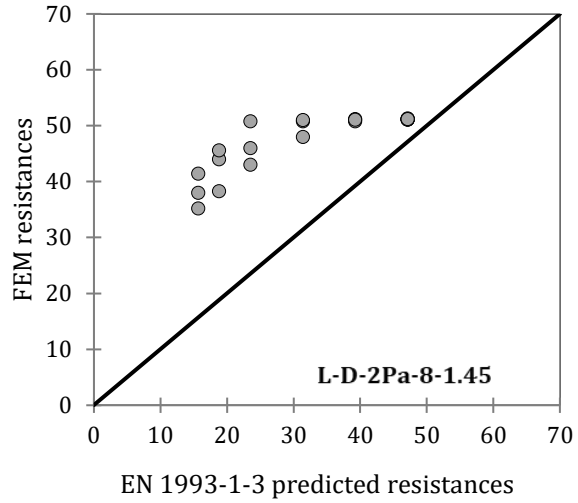
FEM resistances
EN 1993-1-3 predicted resistances
L-D-2Pa-8-1.45

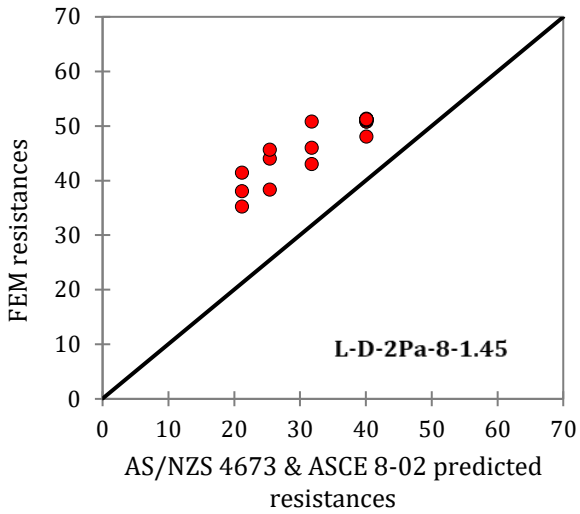
FEM resistances
AS/NZS 4673 & ASCE 8-02 predicted resistances
L-D-2Pa-8-1.45

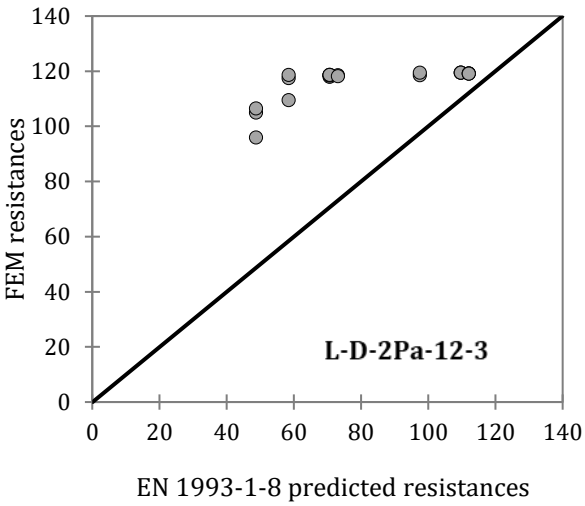
FEM resistances
EN 1993-1-8 predicted resistances
L-D-2Pa-12-3

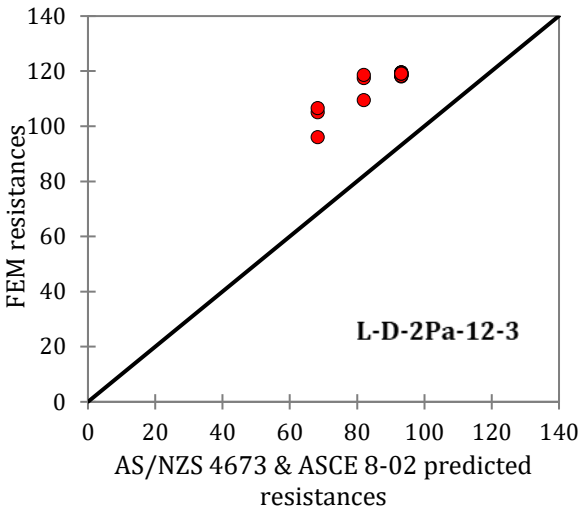
FEM resistances
AS/NZS 4673 & ASCE 8-02 predicted resistances
L-D-2Pa-12-3

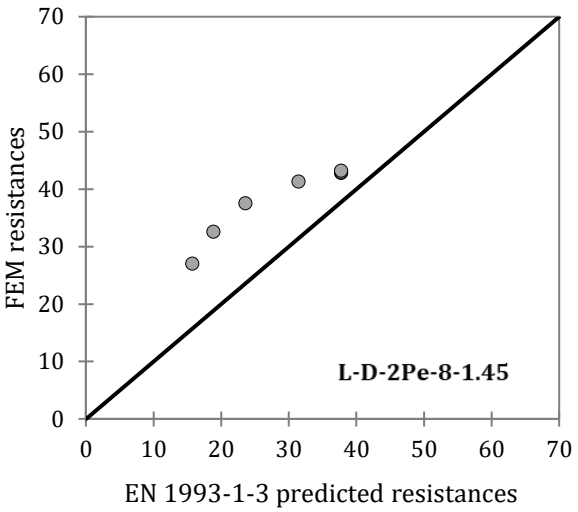
FEM resistances
EN 1993-1-3 predicted resistances
L-D-2Pe-8-1.45

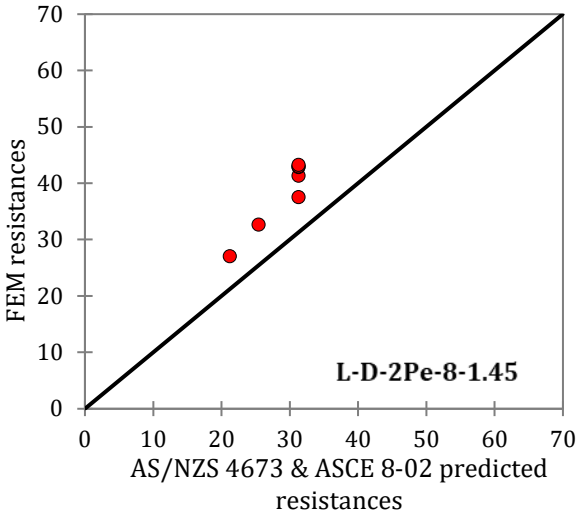
FEM resistances
AS/NZS 4673 & ASCE 8-02 predicted resistances
L-D-2Pe-8-1.45

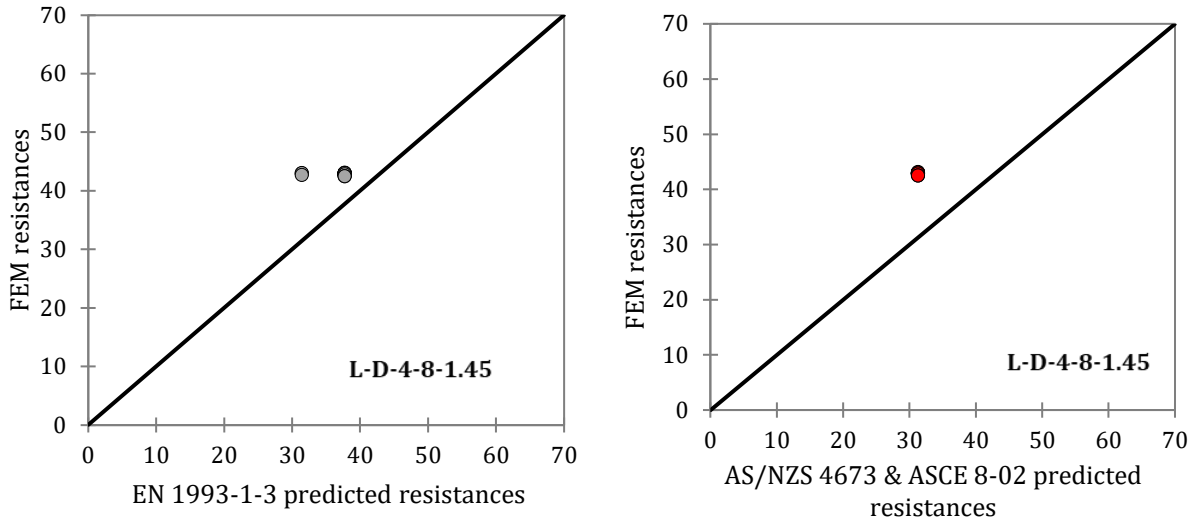

Figure 30 Numerical data versus design prediction data for double shear bolted connections

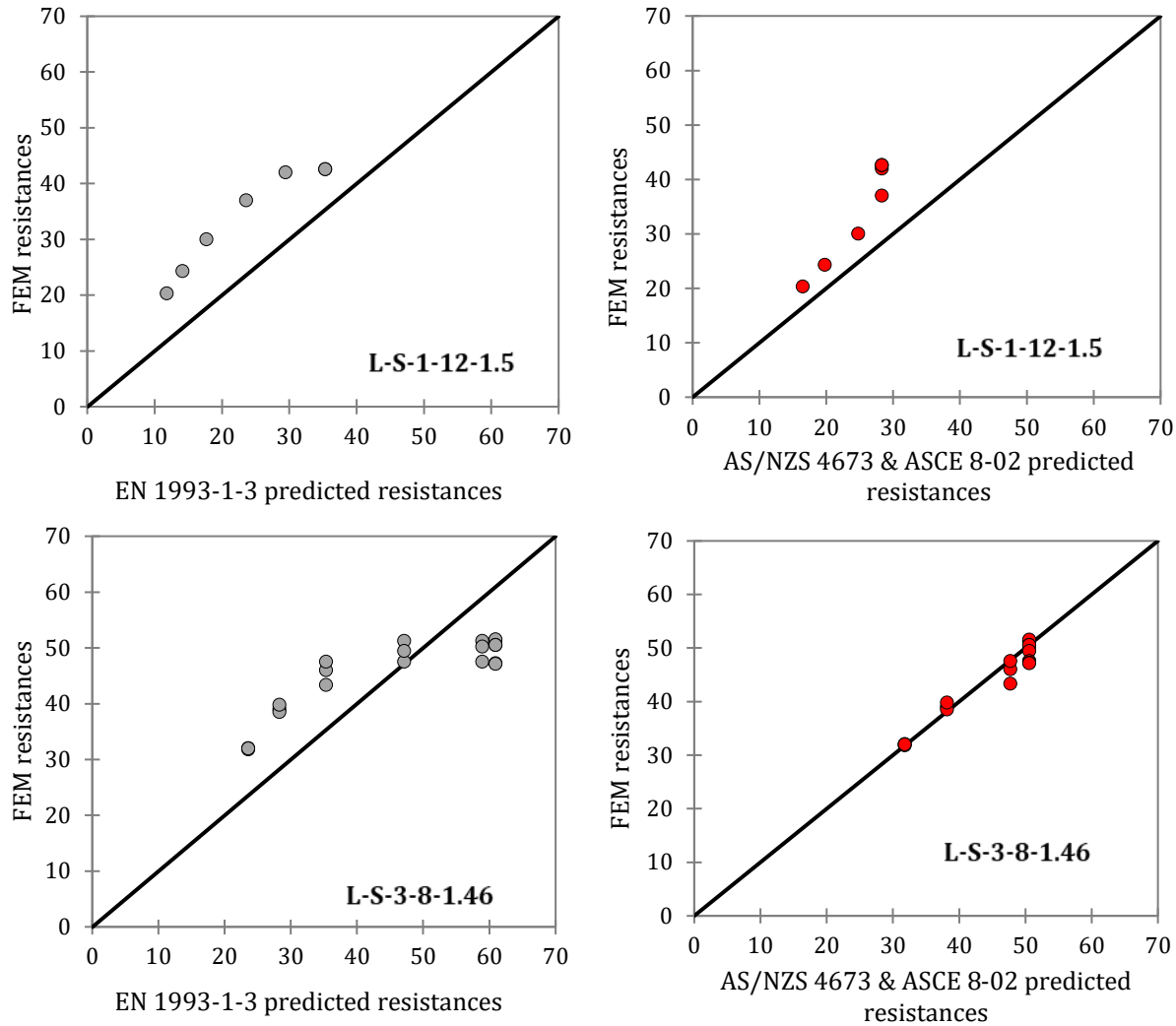

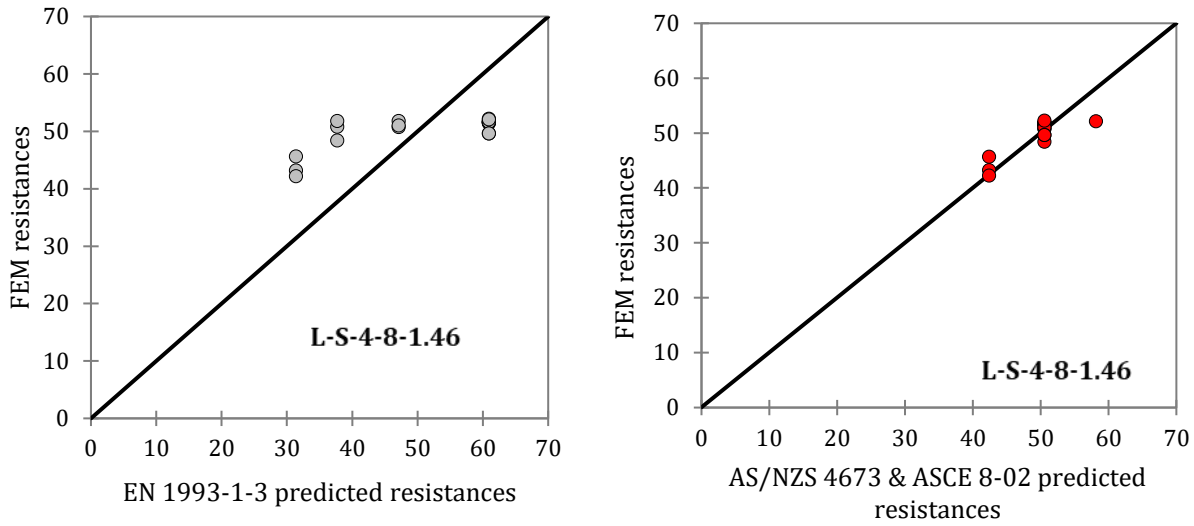

Figure 31 Numerical data versus design prediction data for single shear bolted connections

Following the results of this parametric study and comparative analysis, the following conclusions can be drawn:

- The end ratio e_1/d_0 is the key parameter governing tear out failure. The failure is generally characterized by longitudinal shearing of the plate along two lines tangent to the hole edges in the direction of loading (see Figure 24) or excessive deformation of the plate before fracture occurs at the edges of the bolt hole. In general, this fracture type is found for $e_1/d_0 < 1.2$ and it is more significant in the case of single lap connections. It is also found that this failure mode may be coupled with bearing failure in the cases of double shear connections, depending on the plate thickness and bolt arrangement. Higher thickness of the connection plates and two bolts arrangement in which bolts are arranged parallel to the loading direction prevent its pure shape and early occurring. The AS/NZS Standard [7] and SEI/ASCE Standard [8] can accurately predict tear out capacity using explicit expressions stated in Clause 5.3.1 and 5.3.4, respectively. In contrast, tear out failure is implicitly accounted for in the design bearing resistance formulation in Eurocode 3. To prevent the end tear out mode, SEI/ASCE, AS/NZS and Eurocode 3 should prescribe a lower bound for the e_1/d_0 ratio presently advised to be 1.5 for single shear and 1.2 for double shear.
- When both the end and edge distances are sufficiently large, the bearing fracture is the most critical mode both for single and double shear connections with one bolt arrangement. The localized stress concentration between two distinctly inclined planes followed by considerable pilling-up of material in front of the bolt and excessive hole deformation are the main features of this failure mode (Figure 25). There are currently no design recommendations considering the bolt hole deformability in stainless steel bolted connections in the current specifications. The general equation for bearing failure stated in these codes is only applicable to connections where the deformation around the bolt holes is not a design consideration.
- As it can be seen from Figure 26, net section failure occurs due to stress concentration caused by using more than one bolt perpendicular to the line of action of the load and/or substantial stress concentration at the edge of the bolt hole followed by significant necking at the critical net section (transmission of concentrated localized load by the bolt to the plate material

around). This failure mode is critical for double shear plate connections with four bolt arrangement (the fracture line develops along the internal bolt row of the middle plate) for all considered distance ratios e_1/d_0, e_2/d_0 and p_1/d_0 as well as for double shear connections with two bolts (either perpendicular or parallel to the line of action of the load) with a ratio p_1/d_0 = 2.2. By comparing the single shear connection configuration including four bolts with their double shear counterparts, it can be concluded that the net section efficiency is about 21% higher in the case single shear connections. This could be attributed to the beneficial influence of the lips in the critical cross-section of the external plate where tearing occurs. It should be noted that the lips were designed for the purpose of preventing plate curling in this study.

- The block tearing failure is featured by plate tearing along the perimeter of the holes leading to tearing of a block of material at the end of the connection plate, as it can be seen from Figure 27. The failure mode is influenced by the interaction of shear stresses (parallel to the load) and tensile stresses (perpendicular to the load). This failure appears in single shear bolted connections with three bolts and staggered spacing (more significant), and four bolts arrangement, for a spacing ratio p_1/d_0 = 2.2 (lower bound limit) and end distance ratio e_1/d_0 ranging between 1.5 and 2.5. The design equations stated in the standards [6], [10] are based on the assumption that one of the failure paths is fracture and the other is yielding. However, the specifications for cold-formed structures [7], [8] and [11] do not provide any design expressions to predict block tearing resistance of connections with staggered bolt rows.
- The influence of the variation of the end distance e_1 and spacing p_1 on the ultimate connection capacity is higher for the smaller plate thicknesses (< 3 mm). Considering the double shear connection *L-D-2Pa-8-1.45* (see Figure 28), using a maximum end distance $e_1 = 4t + 40$ increases the ultimate load up to 45% (compared to $e_1 = 1.0d_0$). For the connection type *L-D-2Pa-12-3*, the increase reaches 23%. The influence of the end distance e_1 on the ultimate capacity is higher when the spacing p_1 is minimum i.e., $2.2d_0$.
- The specification codes EN 1993-1-3 [11], EN 1993-1-8 [10], AS/NZS 4673 [7], SEI/ASCE 8-02 [8] quite correctly predict most of the failure modes studied in this research. It is shown that the nominal connection strengths predicted by the AS/NZS and SEI/ASCE specifications are overall more accurate than those predicted by Eurocode 3, as shown in Table A1 and Table A2. Considering the all data for double and single shear bolted connections determined by AS/NZS and SEI/ASCE, the mean values of the numerical-to-predicted load ratio $P_{u,FE}/P_u$ are 1.337 and 1.050, with the corresponding coefficients of variation (CoV) of 0.111 and 0.131, respectively; while the mean values of the numerical-to-predicted load ratio $P_{u,FE}/P_u$ are 1.488 and 1.117, with the corresponding CoV's of 0.254 and 0.256, with Eurocode 3.
- The predicted connections resistances are generally conservative both for the European and Australian/American Specifications, except in the case of net section failure of single shear bolted connections with three and four bolts, and plate thicknesses < 3 mm, see Figure 31. Considering the European code, significant unsafe predictions (i.e., load ratio $P_{u,FE}/P_u$ equal to 0.77) are found for single shear bolted connections with three bolts (staggered bolt spacing), end distance e_1 ranging from $3d_0$ to $4t$+40 and spacing p_1 equal to $5d_0$, see Figure 29. The better

predictions, but still on the unsafe side, are found using equ. (7) of Australian/American Specifications with, for the same distance parameters, a load ratio $P_{u,FE}/P_u$ of 0.93.

4 Conclusions

The behaviour of duplex stainless steel bolted connections has been presented in this paper. The stress-strain curves of duplex stainless steel (EN 1.4462) coupon specimens and load-displacement curves for net cross-section capacity of duplex stainless steel connection plates subjected to tensile loading were presented. Nonlinear finite element (FE) models were developed for duplex stainless steel coupons and connection plates in this study as well as lean duplex stainless steel (EN 1.4162) single shear and double shear bolted connections. The damage model considering ductile damage initiation criterion and damage evolution law was incorporated in the FEMs. It is shown that the numerical simulations can replicate the load-displacement curves, failure modes and ultimate loads of duplex stainless steel coupons and connection plates, and lean duplex stainless steel bolted connections under tensile loading.

An extensive parametric study that consisted of 133 duplex grade EN 1.4162 bolted connection specimens was then performed using the validated FEMs. The failure modes of bolted connections that failed in combined tear out and bearing, bearing and net section due to the effects of end distance, edge distance and spacing between the bolts in the connections, were comprehensively examined. The conclusions of this study are summarized here below:

- Generally, the failure modes obtained from the FEMs could be correctly predicted by the AS/NZS, SEI/ASCE Specification and European codes.
- The AS/NZS, American (SEI/ASCE) Specification and European codes generally provided conservative strength predictions when compared with the numerical strengths, except for those of single shear bolted connections that failed in net section.
- The strengths predicted by the AS/NZS and SEI/ASCE specifications are overall more accurate and less scattered than those predicted by the European codes.
- The influence of the variation of the end distance and bolt spacing in the longitudinal direction on the ultimate strengths is more pronounced for thin plate connections, e.g., up to 45% of strength increase for thicknesses of 1.45 mm compared to 23% for thicknesses of 3.0 mm.
- A lower bound for the e_1/d_0 ratio of 1.5 for single shear and 1.2 for double shear connections is recommended to prevent tear out failure.

5 Acknowledgment

This investigation is supported by the Serbian Ministry of Education, Science and Technological Development through the 200092 project.

Appendix A. Numerical and design load data

Table A1 Comparison of FE strengths with design strengths for double shear bolted connections including duplex stainless steel grade EN 1.4162

							FE parametric study		EN 1993-1-3, EN 1993-1-8		AS/NZS 4673, ASCE 8-02	
FE model / Geometry	t_e (mm)	t_i (mm)	e_1 (mm)	p_1 (mm)	e_2 (mm)	p_2 (mm)	Failure mode	Ultimate load $P_{u,FE}$ (kN)	Predicted failure mode	$P_{u,FE}/P_u$	Predicted failure mode	$P_{u,FE}/P_u$
L-D-1-12-1.5	1.5	1.47	$1.0d_0$ = 14.0	-	25	-	tear out	19.5	bearing	1.65	tear out	1.18
b = 50 mm			$1.2d_0$ = 16.8				bearing	23.5	bearing	1.66	tear out	1.19
$L_{1,e}$ = 381 mm			$1.5d_0$ = 21.0				bearing	29.5	bearing	1.67	tear out	1.19
$L_{1,i}$ = 405 mm			$2.0d_0$ = 28.0				bearing	37.5	bearing	1.59	tear out	1.14
d = 12 mm			$2.5d_0$ = 35.0				bearing	45.0	bearing	1.53	net section	1.28
d_0 = 14 mm			$3.0d_0$ = 42.0				net section	45.2	net section	1.13	net section	1.28
n = 1			$4t$+40 = 45.8				net section	45.5	net section	1.14	net section	1.29
									mean value	1.482	mean value	1.221
									std. deviation	0.241	std. deviation	0.062
									CoV	0.163	CoV	0.050
L-D-1-12-3	3	3	$1.0d_0$ = 14.0	-	30	-	tear out/ bearing	40.0	bearing	1.64	tear out	1.17
b = 60 mm			$1.2d_0$ = 16.8				bearing	48.5	bearing	1.66	tear out	1.18
$L_{1,e}$ = 381 mm			$1.5d_0$ = 21.0				bearing	61.5	bearing	1.68	tear out	1.20
$L_{1,i}$ = 405 mm			$2.0d_0$ = 28.0				bearing	74.0	bearing	1.52	tear out	1.08
d = 12 mm			$2.5d_0$ = 35.0				bearing	86.5	bearing	1.42	bearing	1.07
d_0 = 14 mm			$3.0d_0$ = 42.0				bearing	91.0	bearing	1.26	bearing	1.13
n = 1			$4t$+40 = 52.0				bearing	93.2	bearing	1.29	bearing	1.16
									mean value	1.496	mean value	1.143
									std. deviation	0.174	std. deviation	0.049
									CoV	0.116	CoV	0.043
L-D-2*Pa*-8-1.45	1.45	1.45	$1.0d_0$ = 9.0	$3d_0$ = 27.0	25	-	tear out/ bearing	38.0	bearing	2.42	tear out	1.79
b = 50 mm			$1.2d_0$ = 10.8				bearing	44.0	bearing	2.33	tear out	1.73
$L_{1,e}$ = 386 mm			$1.5d_0$ = 13.5				bearing	46.0	bearing	1.95	tear out	1.45
$L_{1,i}$ = 404 mm			$2.0d_0$ = 18.0				bearing	50.8	bearing	1.62	net section	1.27
d = 8 mm			$2.5d_0$ = 22.5				net section	51.2	bearing	1.30	net section	1.28
d_0 = 9 mm			$3.0d_0$ = 27.0				net section	51.1	net section	1.29	net section	1.27
n = 2			$4t$+40 = 45.8				net section	51.2	net section	1.29	net section	1.28
									mean value	1.743	mean value	1.436

								std. deviation	0.494	std. deviation	0.230
								CoV	0.284	CoV	0.160
L-D-2*Pa*-8-1.45	1.45	1.45	$1.0d_0$ = 9.0	$2.2d_0$ = 19.8	25	-	tear out/ bearing	35.2	bearing	2.24	tear out	1.66
b = 50 mm			$1.2d_0$ = 10.8				bearing	38.3	bearing	2.03	tear out	1.50
$L_{1,e}$ = 386 mm			$1.5d_0$ = 13.5				bearing	43.0	bearing	1.82	tear out	1.35
$L_{1,i}$ = 404 mm			$2.0d_0$ = 18.0				bearing	48.0	bearing	1.53	net section	1.20
d = 8 mm			$2.5d_0$ = 22.5				bearing	50.8	bearing	1.29	net section	1.27
d_0 = 9 mm			$3.0d_0$ = 27.0				net section	51.2	net section	1.29	net section	1.27
n = 2			4*t*+40 = 45.8				net section	51.2	net section	1.29	net section	1.27
									mean value	1.642	mean value	1.361
									std. deviation	0.392	std. deviation	0.164
									CoV	0.239	CoV	0.120
L-D-2*Pa*-8-1.45	1.45	1.45	$1.0d_0$ = 9.0	$5d_0$ = 45.0	25	-	tear out/ bearing	41.4	bearing	2.63	tear out	1.95
b = 50 mm			$1.2d_0$ = 10.8				bearing	45.6	bearing	2.42	tear out	1.79
$L_{1,e}$ = 386 mm			$1.5d_0$ = 13.5				bearing	50.8	bearing	2.15	tear out	1.60
$L_{1,i}$ = 404 mm			$2.0d_0$ = 18.0				bearing/net section	51.0	bearing	1.62	net section	1.27
d = 8 mm			$2.5d_0$ = 22.5				bearing/net section	51.1	bearing	1.30	net section	1.27
d_0 = 9 mm			$3.0d_0$ = 27.0				net section	51.3	net section	1.29	net section	1.28
n = 2			4*t*+40 = 45.8				net section	51.2	net section	1.29	net section	1.28
									mean value	1.816	mean value	1.491
									std. deviation	0.577	std. deviation	0.289
									CoV	0.318	CoV	0.194
L-D-2*Pa*-12-3	3	3	$1.0d_0$ = 14.0	$3d_0$ = 42.0	30	-	tear out/bearing	105.0	bearing	2.15	tear out	1.54
b = 60 mm			$1.2d_0$ = 16.8				bearing	117.5	bearing	2.01	tear out	1.43
$L_{1,e}$ = 386 mm			$1.5d_0$ = 21.0				net section	118.5	bearing	1.62	net section	1.27
$L_{1,i}$ = 404 mm			$2.0d_0$ = 28.0				net section	118.5	bearing	1.21	net section	1.27
d = 12 mm			$2.5d_0$ = 35.0				net section	119.5	net section	1.18	net section	1.28
d_0 = 14 mm			$3.0d_0$ = 42.0				net section	119.4	net section	1.18	net section	1.28
n = 2			4*t*+40 = 52.0				net section	119.4	net section	1.18	net section	1.28
									mean value	1.506	mean value	1.337
									std. deviation	0.424	std. deviation	0.106
									CoV	0.282	CoV	0.079
L-D-2*Pa*-12-3	3	3	$1.0d_0$ = 14.0	$2.2d_0$ = 30.8	30	-	tear out/bearing	96.0	bearing	1.97	tear out	1.41
b = 60 mm			$1.2d_0$ = 16.8				bearing	109.5	bearing	1.87	tear out	1.34

$L_{1,e}$ = 386 mm			$1.5d_0$ = 21.0				bearing/net section	118.0	bearing	1.67	net section	1.27
$L_{1,i}$ = 404 mm			$2.0d_0$ = 28.0				bearing/net section	118.4	bearing	1.67	net section	1.27
d = 12 mm			$2.5d_0$ = 35.0				net section	118.6	bearing	1.68	net section	1.27
d_0 = 14 mm			$3.0d_0$ = 42.0				net section	118.6	bearing	1.68	net section	1.27
n = 2			$4t$+40 = 52.0				net section	118.6	bearing	1.68	net section	1.27
									mean value	1.744	mean value	1.300
									std. deviation	0.123	std. deviation	0.053
									CoV	0.070	CoV	0.040
L-*D*-2*Pa*-12-3	3	3	$1.0d_0$ = 14.0	$5d_0$ = 70.0	30	-	tear out/bearing	106.5	net section	2.18	tear out	1.56
b = 60 mm			$1.2d_0$ = 16.8				bearing	118.6	net section	2.03	tear out	1.45
$L_{1,e}$ = 386 mm			$1.5d_0$ = 21.0				net section	118.2	net section	1.62	net section	1.27
$L_{1,i}$ = 404 mm			$2.0d_0$ = 28.0				net section	119.5	net section	1.22	net section	1.28
d = 12 mm			$2.5d_0$ = 35.0				net section	119.2	net section	1.18	net section	1.28
d_0 = 14 mm			$3.0d_0$ = 42.0				net section	119.1	net section	1.18	net section	1.28
n = 2			$4t$+40 = 52.0				net section	119.1	net section	1.18	net section	1.28
									mean value	1.513	mean value	1.342
									std. deviation	0.436	std. deviation	0.115
									CoV	0.288	CoV	0.086
L-*D*-2*Pe*-8-1.45	1.45	1.47	$1.0d_0$ = 9.0	-	14	$2.4d_0$ = 22	tear out	27.0	bearing	1.72	tear out	1.27
b = 50 mm			$1.2d_0$ = 10.8				bearing	32.6	bearing	1.73	tear out	1.28
$L_{1,e}$ = 375 mm			$1.5d_0$ = 13.5				bearing/net section	37.5	bearing	1.59	net section	1.20
$L_{1,i}$ = 390 mm			$2.0d_0$ = 18.0				net section	41.3	bearing	1.35	net section	1.32
d = 8 mm			$2.5d_0$ = 22.5				net section	42.8	net section	1.20	net section	1.37
d_0 = 9 mm			$3.0d_0$ = 27				net section	42.9	net section	1.14	net section	1.37
n = 2			$4t$+40 = 45.8				net section	43.2	net section	1.15	net section	1.38
									mean value	1.410	mean value	1.312
									std. deviation	0.265	std. deviation	0.067
									CoV	0.188	CoV	0.051
L-*D*-4-8-1.45	1.45	1.45	$1.0d_0$ = 9.0	$3.0d_0$ = 27.0	14	$2.4d_0$ = 22	net section	43.0	bearing	1.37	net section	1.37
b = 50 mm			$1.2d_0$ = 10.8				net section	43.1	net section	1.14	net section	1.38
$L_{1,e}$ = 386 mm			$1.5d_0$ = 13.5				net section	42.9	net section	1.14	net section	1.37
$L_{1,i}$ = 404 mm			$2.0d_0$ = 18.0				net section	42.8	net section	1.13	net section	1.37
d = 8 mm			$2.5d_0$ = 22.5				net section	42.8	net section	1.13	net section	1.37
d_0 = 9 mm			$3.0d_0$ = 27				net section	42.8	net section	1.13	net section	1.36
n = 4			$4t$+40 = 45.8				net section	42.7	net section	1.13	net section	1.36

									mean value	1.169	mean value	1.368
									std. deviation	0.087	std. deviation	0.004
									CoV	0.075	CoV	0.003
L-*D*-4-8-1.45	1.45	1.45	$1.0d_0$ = 9.0	$2.2d_0$ = 19.8	14	$2.4d_0$ = 22	net section	43.0	bearing	1.37	net section	1.37
b = 50 mm			$1.2d_0$ = 10.8				net section	42.8	net section	1.13	net section	1.37
$L_{1,e}$ = 386 mm			$1.5d_0$ = 13.5				net section	42.8	net section	1.13	net section	1.37
$L_{1,i}$ = 404 mm			$2.0d_0$ = 18.0				net section	42.8	net section	1.13	net section	1.37
d = 8 mm			$2.5d_0$ = 22.5				net section	42.9	net section	1.14	net section	1.37
d_0 = 9 mm			$3.0d_0$ = 27				net section	42.9	net section	1.14	net section	1.37
n = 4			4*t*+40 = 45.8				net section	42.9	net section	1.14	net section	1.37
									mean value	1.169	mean value	1.369
									std. deviation	0.088	std. deviation	0.002
									CoV	0.075	CoV	0.002
L-*D*-4-8-1.45	1.45	1.45	$1.0d_0$ = 9.0	$5d_0$ = 45.0	14	$2.4d_0$ = 22	net section	42.7	bearing	1.36	net section	1.36
b = 50 mm			$1.2d_0$ = 10.8				net section	43.0	net section	1.14	net section	1.37
$L_{1,e}$ = 386 mm			$1.5d_0$ = 13.5				net section	43.0	net section	1.14	net section	1.37
$L_{1,i}$ = 404 mm			$2.0d_0$ = 18.0				net section	43.0	net section	1.14	net section	1.37
d = 8 mm			$2.5d_0$ = 22.5				net section	42.8	net section	1.13	net section	1.37
d_0 = 9 mm			$3.0d_0$ = 27				net section	42.5	net section	1.13	net section	1.36
n = 4			4*t*+40 = 45.8				net section	42.5	net section	1.13	net section	1.36
									mean value	1.167	mean value	1.366
									std. deviation	0.085	std. deviation	0.007
									CoV	0.073	CoV	0.005

Table A2 Comparison of FE strengths with design strengths for single shear bolted connections including duplex stainless steel grade EN 1.4162

						FE parametric study		EN 1993-1-3, EN 1993-1-8		AS/NZS 4673, ASCE 8-02	
FE model / Geometry	t_e (mm)	e_1 (mm)	p_1 (mm)	e_2 (mm)	p_2 (mm)	Failure mode	Ultimate load $P_{u,FE}$ (kN)	Predicted failure mode	$P_{u,FE}/P_u$	Predicted failure mode	$P_{u,FE}/P_u$
L-*S*-1-12-1.5	1.5	$1.0d_0$ = 14.0	-	25	-	tear out	20.3	bearing	1.72	tear out	1.23
b = 50 mm		$1.2d_0$ = 16.8				tear out	24.3	bearing	1.72	tear out	1.23
$L_{1,e}$ = 381 mm		$1.5d_0$ = 21.0				bearing	30.0	bearing	1.70	tear out	1.21
d = 12 mm		$2.0d_0$ = 28.0				bearing	37.0	bearing	1.57	bearing	1.31
d_0 = 14 mm		$2.5d_0$ = 35.0				bearing	42.0	bearing	1.43	bearing	1.48
n = 1		$3.0d_0$ = 42.0				bearing	42.6	bearing	1.20	bearing	1.51
		$4t$+40 = 45.8				bearing	42.6	bearing	1.20	bearing	1.51
								mean value	1.506	mean value	1.353
								std. deviation	0.231	std. deviation	0.140
								CoV	0.153	CoV	0.103
L-*S*-3-8-1.46	1.46	$1.0d_0$ = 9.0	$3.0d_0$ = 27.0	14	$2.4d_0$ = 22	tear out	31.8	bearing	1.35	tear out	1.00
b = 50 mm		$1.2d_0$ = 10.8				tear out	39.0	bearing	1.38	tear out	1.02
$L_{1,e}$ = 386 mm		$1.5d_0$ = 13.5				bearing	46.0	bearing	1.30	tear out	0.96
d = 8 mm		$2.0d_0$ = 18.0				bearing	51.2	bearing	1.09	net section	1.01
d_0 = 9 mm		$2.5d_0$ = 22.5				net section	51.2	bearing	0.87	net section	1.01
n = 3		$3.0d_0$ = 27.0				net section	51.3	net section	0.84	net section	1.01
		$4t$+40 = 45.8				net section	51.5	net section	0.84	net section	1.02
								mean value	1.095	mean value	1.005
								std. deviation	0.247	std. deviation	0.020
								CoV	0.225	CoV	0.020
L-*S*-3-8-1.46	1.46	$1.0d_0$ = 9.0	$2.2d_0$ = 19.8	14	$2.4d_0$ = 22	tear out	32.0	bearing	1.36	tear out	1.01
b = 50 mm		$1.2d_0$ = 10.8				tear out	38.5	bearing	1.36	tear out	1.01
$L_{1,e}$ = 386 mm		$1.5d_0$ = 13.5				block tearing	43.3	bearing	1.22	tear out	0.91
d = 8 mm		$2.0d_0$ = 18.0				block tearing	47.5	bearing	1.01	net section	0.94
d_0 = 9 mm		$2.5d_0$ = 22.5				block tearing	50.2	bearing	0.85	net section	0.99
n = 3		$3.0d_0$ = 27.0				net section	50.5	net section	0.83	net section	1.00
		$4t$+40 = 45.8				net section	50.5	net section	0.83	net section	1.00
								mean value	1.066	mean value	0.978
								std. deviation	0.245	std. deviation	0.039
								CoV	0.230	CoV	0.040

L-*S*-3-8-1.46	1.46	$1.0d_0$ = 9.0	$5d_0$ = 45.0	14	$2.4d_0$ = 22	tear out	32.0	bearing	1.36	tear out	1.00
b = 50 mm		$1.2d_0$ = 10.8				tear out	39.8	bearing	1.41	tear out	1.04
$L_{1,e}$ = 386 mm		$1.5d_0$ = 13.5				bearing	47.5	bearing	1.34	tear out	0.99
d = 8 mm		$2.0d_0$ = 18.0				net section	49.4	bearing	1.05	net section	0.98
d_0 = 9 mm		$2.5d_0$ = 22.5				net section	47.5	bearing	0.81	net section	0.94
n = 3		$3.0d_0$ = 27.0				net section	47.2	net section	0.77	net section	0.93
		$4t$+40 = 45.8				net section	47.1	net section	0.77	net section	0.93
								mean value	1.072	mean value	0.974
								std. deviation	0.293	std. deviation	0.042
								CoV	0.273	CoV	0.044
L-*S*-4-8-1.46	1.46	$1.0d_0$ = 9.0	$3.0d_0$ = 27.0	14	$2.4d_0$ = 22	tear out	43.2	bearing	1.37	tear out	1.02
b = 50 mm		$1.2d_0$ = 10.8				tear out	50.8	bearing	1.35	tear out	1.00
$L_{1,e}$ = 386 mm		$1.5d_0$ = 13.5				bearing	51.8	bearing	1.10	net section	1.02
d = 8 mm		$2.0d_0$ = 18.0				net section	51.8	net section	0.85	net section	1.02
d_0 = 9 mm		$2.5d_0$ = 22.5				net section	51.5	net section	0.84	net section	1.02
n = 4		$3.0d_0$ = 27.0				net section	51.7	net section	0.85	net section	1.02
		$4t$+40 = 45.8				net section	51.7	net section	0.85	net section	1.02
								mean value	1.031	mean value	1.018
								std. deviation	0.243	std. deviation	0.007
								CoV	0.236	CoV	0.007
L-*S*-4-8-1.46	1.46	$1.0d_0$ = 9.0	$2.2d_0$ = 19.8	14	$2.4d_0$ = 22	tear out	42.2	bearing	1.34	tear out	0.99
b = 50 mm		$1.2d_0$ = 10.8				block tearing	48.4	bearing	1.28	tear out	0.96
$L_{1,e}$ = 386 mm		$1.5d_0$ = 13.5				net section	50.7	bearing	1.08	net section	1.00
d = 8 mm		$2.0d_0$ = 18.0				net section	51.4	net section	0.84	net section	1.02
d_0 = 9 mm		$2.5d_0$ = 22.5				net section	51.6	net section	0.85	net section	1.02
n = 4		$3.0d_0$ = 27.0				net section	51.7	net section	0.85	net section	1.02
		$4t$+40 = 45.8				net section	51.7	net section	0.85	net section	1.02
								mean value	1.013	mean value	1.004
								std. deviation	0.222	std. deviation	0.023
								CoV	0.219	CoV	0.023
L-*S*-4-8-1.46	1.46	$1.0d_0$ = 9.0	$5d_0$ = 45.0	14	$2.4d_0$ = 22	tear out	45.7	bearing	1.45	tear out	1.08
						bearing/net		bearing	1.37	tear out	1.02
b = 50 mm		$1.2d_0$ = 10.8				section	51.8				
$L_{1,e}$ = 386 mm		$1.5d_0$ = 13.5				net section	51.0	bearing	1.08	net section	1.01
d = 8 mm		$2.0d_0$ = 18.0				net section	49.6	net section	0.81	net section	0.98

d_0 = 9 mm n = 4	$2.5d_0$ = 22.5 $3.0d_0$ = 27.0 $4t$+40 = 45.8	net section net section net section	49.6 52.2 52.1	net section net section net section mean value std. deviation CoV	0.81 0.86 0.86 1.036 0.274 0.264	net section net section net section mean value std. deviation CoV	0.98 1.03 1.03 1.018 0.033 0.033

6 Bibliography

[1]. Outokumpu Stainless AB. Handbook of Stainless Steel. Avesta: Outokumpu Oyj. 2013.

[2]. EN 10088. Stainless steels Part 2: Technical delivery conditions for sheet/plate and strip of corrosion resisting steels for general purposes. EN 10088-2: 2014.

[3]. G. Gedge. Structural uses of stainless steel - buildings and civil engineering. Journal of Constructional Steel Research, 64 (11) (2008), pp. 1194-1198.

[4]. N.R. Baddoo, A. Kosmač, Sustainable Duplex Stainless Steel Bridges. United Kingdom, Brussels. 2010.

[5]. EN 1993-1-4. Eurocode 3: Design of steel structures - Part 1.4: General rules - Supplementary rules for stainless steel. 2006.

[6]. AISC: Specification for structural steel buildings. AISC 360. Chicago: AISC 2016.

[7]. AS/NZS 4673:2001: Cold-formed stainless steel structures. Australian – New Zealand Standard. Standards Australia, 2001.

[8]. SEI/ASCE 8-02: Specification for the Design of Cold-Formed Stainless Steel Structural Members, American Society of Civil Engineers, 2002.

[9]. NBN EN 20273 - ISO 273: Fasteners-Clearance holes for bolts and screws. 1992.

[10]. EN 1993-1-8. Eurocode 3: Design of steel structures - Part 1-8: Design of joints. 2005.

[11]. EN 1993-1-3. Eurocode 3: Design of Steel Structures – Part 1-3: General rules - Supplementary rules for cold-formed members and sheeting EN 1993-1-3, Brussels, Belgium, 2006.

[12]. ASTM F3125. Standard Specification for High Strength Structural Bolts, Steel and Alloy Steel, Heat Treated, 120 ksi (830 MPa) and 150 ksi (1040 MPa) Tensile Strength, Inch and Metric Dimensions. ASTM International.

[13]. EN ISO 3506-1. Mechanical properties of corrosion-resistant stainless steel fasteners - Part 1 : Bolts, screws and studs. Brussels, Belgium, CEN 2009.

[14]. Design Manual for Structural Stainless Steel: Part 1 - Recommendations. Silwood Park, Ascot, Berkshire, SL5 7QN, UK: SCI.

[15]. E.L. Salih, L. Gardner, N.A. Nethercot. Numerical investigation of net section failure in stainless steel bolted connections. Journal of Constructional Steel Research, 66(12) (2010), pp. 1455–1466.

[16]. E.L. Salih, L. Gardner, N.A. Nethercot. Bearing failure in stainless steel bolted connections. Engineering Structures, 33 (2) (2011), pp. 549–562.

[17]. G. Kiymaz. Investigations on the bearing strength of stainless steel bolted plates under in-plane tension. Steel and Composite Structures, 9 (2) (2009), pp. 173-189.

[18]. A. Talja, M. Torkar. Lap shear tests of bolted and screwed ferritic stainless steel connections. Thin-Walled Structures, 83 (2014), pp. 157-168.

[19]. Y. Cai, B. Young. Structural behaviour of cold-formed stainless steel bolted connections. Thin-Walled Structures, 83 (2014), pp. 147-156.

[20]. Y. Cai, B. Young. Behaviour of cold-formed stainless steel single shear bolted connections at elevated temperatures. Thin-Walled Structures, 75 (2014), pp. 63-75.

[21]. Y. Cai, B. Young. High temperature tests of cold-formed stainless steel double shear bolted connections. Journal of Constructional Steel Research, 104 (2015), pp. 49-63.

[22]. Y. Cai, B. Young. Bearing factors of cold-formed stainless steel double shear bolted connections at elevated temperatures. Thin-Walled Structures, 98 (A) (2016), pp. 212-229.

[23]. Y. Cai, B. Young. Fire resistance of stainless steel single shear bolted connections, Thin-Walled Structures, 130 (2018), pp. 332-346.

[24]. Y. Cai, B. Young. Transient state tests of cold-formed stainless steel single shear bolted connections. Engineering Structures, 81 (2014), pp. 1-9.

[25]. T.S. Kim, J. Lim. Ultimate Strength of Single Shear Two-bolted Connections with Austenitic Stainless Steel. International Journal of Steel Structures, 13 (2013), pp. 117-128.

[26]. A. Bouchaïr, J. Averseng, A. Abidelah. Analysis of the behaviour of stainless steel bolted connections. Journal of Constructional Steel Research, 64 (11) (2008), pp. 1264–1274.

[27]. Y. Song, J., Wang, B. Uy, D. Li. Experimental behaviour and fracture prediction of austenitic stainless steel bolts under combined tension and shear, Journal of Constructional Steel Research, 166 (2020), 105916.

[28]. H.X. Yuan, S. Hu, X.X. Du, L. Yang, X.Y. Cheng, M. Theofanous. Experimental behaviour of stainless steel bolted T-stub connections under monotonic loading, Journal of Constructional Steel Research, 152 (2019), pp. 213-224.

[29]. JGJ 82, Technical Specification for High Strength Bolt Connections of Steel Structures, China Architecture and Building Press, Beijing, 2011 (in Chinese).

[30]. H.X. Yuan, J.D. Gao, M. Theofanous, L. Yang, B.W. Schafer, Initial stiffness and plastic resistance of bolted stainless steel T-stubs in tension, Journal of Constructional Steel Research, 173 (2020), pp. 1-14.

[31]. MatchID www.matchid.eu

[32]. ABAQUS User Manual, Version 6.12, Providence RI, USA: DS SIMULIA Corp (2012).

[33]. ISO 262. ISO general purpose metric screw threads — Selected sizes for screws, bolts and nuts. International Organization for Standardization, Geneva, Switzerland, 1998.

[34]. Y. Hu, L. Shen, S. Nie, B. Yang, W. Sha, FE simulation and experimental tests of high-strength structural bolts under tension. Journal of Constructional Steel Research, 126 (2016) pp. 174-186

[35]. ISO 6892-1: Metallic materials -Tensile testing - Part 1: Method of test at room temperature. 2009.

[36]. I. Arrayago, E. Real, L. Gardner, Description of stress-strain curves for stainless steel alloys, Materials and Design, 87 (2015) pp. 540-552.

[37]. M. Pavlović, Z. Marković Z, M. Veljković, D. Buđevac, Bolted shear connectors vs. headed studs behavior in push-out tests. Journal of Constructional Steel Research, 88 (2013) pp. 134-149.

[38]. J. Dobrić, D. Budjevac, Z. Marković, N. Gluhović, Behaviour of stainless steel press-braked channel sections under compression, Journal of Constructional Steel Research, 139 (2017) pp. 236-253.

[39]. G. Trattnig, T. Antretter, R. Pippan, Fracture of austenitic steel subject to a wide range of stress triaxiality ratios and crack deformation modes, Eng. Fract. Mech. 75 (2) (2008) 223–235.

[40]. J.R. Rice, D.M. Tracey, On the Ductile Enlargement of Voids in Triaxial Stress Fields, J. Mechanics and Phys. Solids 17 (1969) 201–217.

[41]. J.A. Lemaitre, Continuous Damage Mechanics Model for Ductile Fracture, J. Eng. Mater. Technol. 107 (1) (1985) 83–90.

[42]. M. Pavlović, C. Heistermann, M. Veljković, D. Pak, M. Feldmann, C. Rebelo, L. Simões da Silva, Connections in towers for wind converters, part I: Evaluation of down-scaled experiments, Journal of Constructional Steel Research, 115 (2015) 445-457.

[43]. M. Pavlović, C. Heistermann, M. Veljković, D. Pak, M. Feldmann, C. Rebelo, L. Simões da Silva, Connections in towers for wind converters, Part II: The friction connection behaviour, Journal of Constructional Steel Research, 115 (2015) 458-466.

[44]. M. Pavlović, C. Heistermann, M. Veljković, D. Pak, M. Feldmann, C. Rebelo, L. Simões da Silva, Friction connection vs. ring flange connection in steel towers for wind converters, Engineering Structures, 98 (2015) 151-162.

[45]. Rules on high strength steel (RUOSTE), Final report, European Commission, Research Fund for Coal and Steel, Grant Agreement RFSR-CT-2012-00036, 1 July 2012 – 30 June 2015.